DESIGN OF ADAPTIVE CONTROLLER AND EXTREMUM SEEKING ALGORITHM FOR QUADROTORS

by

Hüseyin Demircioğlu

B.S., Mechanical Engineering, Boğaziçi University, 2013

Submitted to the Institute for Graduate Studies in
Science and Engineering in partial fulfillment of
the requirements for the degree of
Master of Science

Graduate Program in Mechanical Engineering

Boğaziçi University

2018

ACKNOWLEDGEMENTS

This work was supported by the Boğaziçi Scientific Research Projects (BAP, 10341). I would like to express my gratitude to my supervisor Assist. Prof. Halil İbrahim Baştürk whom I thank very deeply to have given me a chance, and to have me guided, supported and encouraged throughout my master period. Also, I would like to thank Assist Prof. Evren Samur and Assoc. Prof. Erdinç Altuğ for their participation to my thesis committee.

I would like to convey my thanks to Erdem Arinç Bulgur for his participation in my thesis and being a lab friend. Furthermore, I would like thank to Uğur Alican Alma, Engin Kılıç, İbrahim Ulaş Özturan, Gökalp Sönmez and Recep Özgür Uzun for always making me feel that I will never walk alone and to Cem Sinan Öztürk for his precious friendship and advices.

Lastly, I want to take this opportunity to express my heartiest gratitude; to my parents Hediye and Bülent Demircioğlu, my other parents Birsel and Murat Demircioğlu, my siblings İsmet Ertuğrul Demircioğlu, Duhan Hopurcuoğlu, Sare Kaya and Nihan Saka for their blessing, unwavering support, encouragement and trust through my all life and I would like to thank to my uncle Prof. Ahmet Coşkun Sönmez for his being a role model for me. This accomplishment would not have been possible without them.

ABSTRACT

DESIGN OF ADAPTIVE CONTROLLER AND EXTREMUM SEEKING ALGORITHM FOR QUADROTORS

In this thesis, two tasks for quadrotors are presented. The first is an inner and the second is an outer loop control design for quadrotors.

For the first task, an adaptive contoller for quadrotors is designed. During the design, it is assumed that all system parameters are unknown. Moreover, the wind disturbances are assumed as a finite sum of sinusoidal functions with unknown frequencies, amplitudes and phases. It is proved that the equilibrium of the closed loop error system is stable, all signals are bounded and desired altitude and attitude control are achieved despite unknown wind disturbances and plant parameters. A simulation is performed to show the feasibility of the design. The advantage of the designed controller is shown by comparing with PID controller in an experimental setup

For the second task, extremum seeking control theory is used. This theory enables to find the closest minimum or the closest maximum from a starting point in a function without having any foreknowledge about the function. In the experiment, this function refers to a nonlinear signal map created by a light source and it decays down from the source. The quadrotor has the ability of measuring the lux value in this signal map by a luminosity sensor. It measures the lux values in a circular line around itself as it is anchored to the floor. By using the measured value, extremum seeking is performed and the quadrotor is steered to the maximum lux value point (the front of the light source) on the circular line where the light sensor can travel on.

ÖZET

DÖRT ROTORLU İNSANSIZ HAVA ARACI İÇİN UYARLAMALI KONTROLCÜ VE EKSTREMUM ARAMA ALGORİTMASI TASARIMI

Bu tezde dörtlü rotorlu insansız hava aracı için iki amaç sunulmuştur. Birincisi iç döngü ve ikincisi dış döngü kontrol tasarımıdır.

Birinci amaç için, dört rotorlu insansız hava araçları için uyarlamalı kontrolcü tasarlanmıştır. Tasarım sırasında, tüm sistem parametrelerinin bilinmediği varsayılmaktadır. Rüzgarın araç üzerindeki bozucu etkisi bilinmeyen frekans, genlik ve fazlara sahip sınırlı sayıdaki sinüzoidal fonksiyonların toplamı olarak varsayılmıştır. Kapalı çevrim sisteminin kararlı olduğu, tüm sinyallerin sınırlı oldugu ve bilinmeyen bozucu rüzgar etkisi ve sistem parametrelerine rağmen arzu edilen davranış ve irtifa kontrolünün elde edildigi kanıtlanmıştır. Tasarımın fizibilitesini göstermek için bir benzetim sunulmuştur. Tasarlanan kontrolcü, bir deney düzeneğinde OIT (Oran-İntegral-Türev) kontrolcüsüyle karşılaştırılarak, avantajı gösterildi.

İkinci amaç için, ekstremum arama kontrol teorisi kullanılmıştır. Bu teori, fonksiyon hakkında herhangi bir bilgi olmadan, başlangıç noktasına en yakın maksimum ya da minimumu bulmayı sağlar. Deneyde, bu fonksiyon, bir ışık kaynağı tarafından oluşturulan doğrusal olmayan bir sinyal haritasını ifade eder ve kaynaktan uzaklaştıkça azalır. Araç, bu sinyal haritasındaki lüks değerini bir ışık sensörü ile ölçme yeteneğine sahiptir. Araç zemini sabitlendiği için, kendi etrafında bulunan dairesel hattaki lüks değerlerini ölçer. Ölçülen değeri kullanarak, ekstremum arayışı gerçekleştirilir ve araç, ışık sensörünün hareket edebileceği dairesel hat üzerindeki maksimum lüks değer noktasına (ışık kaynağının önü) yönlendirilir.

TABLE OF CONTENTS

ACKNOWLEDGEMENTS iii
ABSTRACT iv
ÖZET v
LIST OF FIGURES vii
LIST OF TABLES ix
LIST OF SYMBOLS x
LIST OF ACRONYMS/ABBREVIATIONS xi
1. INTRODUCTION 1
1.1. Literature 1
1.2. Purpose 5
2. SYSTEM MODELING 7
2.1. Kinematic Model 7
2.2. Equations of Motions 8
2.3. Wind Disturbance 10
3. ADAPTIVE CONTROLLER DESIGN AND RESULTS 12
3.1. Wind Disturbance Observer 12
3.2. Controller Design 16
3.3. Stability Proof 21
3.4. Simulation Results 24
3.5. Experimental Results 29
4. EXTREMUM SEEKING CONTROLLER DESIGN 32
4.1. Controller Algorithm 32
4.2. Experimental Setup 38
4.3. Result 41
5. CONCLUSION 45
REFERENCES 46
APPENDIX A: WIND DISTURBANCE CALCULATION 52
APPENDIX B: ERROR DYNAMICS 53

LIST OF FIGURES

Figure 1.1. Basic movements of a quadrotor 3

Figure 2.1. Scheme of quadrotor. The blue lines represents the wind velocity vector at 5 nodes defined on the quadrotor. 7

Figure 3.1. Wind velocity vs time at the position (1,1,1) with respect to EFF 26

Figure 3.2. MATLAB simulation results. 27

Figure 3.3. Angular velocities of rotors vs Time 28

Figure 3.4. Experimental setup for the comparison between the performances of PID and the designed adaptive controller. 29

Figure 3.5. Results of the experiment. 31

Figure 4.1. Scheme of the quadrotor 33

Figure 4.2. Extremum seeking control loop 34

Figure 4.3. Setup of the experiment 39

Figure 4.4. Equipments used for the Extremum Seeking 40

Figure 4.5. System configuration diagram 41

Figure 4.6. Experimental results for the light source tracking of the quadrotor 43

Figure 4.7. Extremum seeking experiment in a basketball field 44

LIST OF TABLES

Table 3.1. Parameter Values Used in Simulations 25

Table 3.2. Root Mean Square Error Comparison 30

LIST OF SYMBOLS

A	Surface area of quadrotor
B_1, B_2, B_3	Axis of body fixed frame
b	Thrust factor of propeller
C_D	Drag coefficient
d	Drag factor of propeller
E_1, E_2, E_3	Axis of earth fixed frame
g	Gravity
J	Principal moment of inertia
M	Wind moment
m	Mass of quadrotor
l	Length of quadrotor's arm
U	Wind force
V	Wind velocity
ϕ	Roll angle
θ	Pitch angle
ψ	Yaw angle
ω	Angular velocity of quadrotor
Ω	Angular velocity of rotor
ν	Wind disturbation
ψ_s	Yaw angle of sensor

LIST OF ACRONYMS/ABBREVIATIONS

UAV	Unmanned aerial vehicle
VTOL	Vertical take-off and landing
BFF	Body fixed frame
EFF	Earth fixed frame
IMU	Inertial measurement unit

1. INTRODUCTION

1.1. Literature

Unmanned aerial vehicle (UAV) was first used by the United States in 1916 during the First World War [1]. However, the lack of sufficient theoretical accumulation in the control area and the fact that existing communication and calculation technology is not able to capture the level to support such projects, it could not be further developed until the end of the war. Early-stage vehicles were controlled by a trained staff from an on-site command center [2]. With the progress of the technology and, in particular, the development of the control theory, autonomous UAVs have been designed since the beginning of the 1960's and it was intensely used in military applications [3]. Considering not risking the safety of trained individuals, the military field has increased the importance of the UAV since 1980s as it can be used in intelligence gathering, mapping creating patrols and, if necessary, deploying weapons and defense-attack features [4].

Initially, fixed-wing type of UAVs was used mainly. However, due to the spread of civilian usage at the beginning in 2000 , different types of design have appeared. Of these design types, the most common one is quadrotor (known as quadcopter) which is classified as rotary wings with four-rotor and has ability of vertical take-off and landing (VTOL) [5]. The structure of quadrotors is simpler than the one of fixed-wing vehicles. Also, there are many other advantages of quadrotors like small in size, able to vertical takeoff and landing, having high maneuverability and simple structure and low-cost. However, beside its simpler structure, its control is harder due to its complex dynamics and fixed wing UAVs are more preferable in long-term and high-altitude military or civilian mission due to their long and quiet flight capability, heavy cargo carrying capacity and their durable physical structure.

Quadrotors are nowadays widely used for mainly video and photo shoots in areas where people are unable to reach [6]. The world's leading e-commerce firm, Amazon, plans to use quadrotors to ship products to buyer in a faster way. Besides this type of

use, quadrotors offer very important opportunities for search-and-rescue and routine security patrol in unreachable places [7]. In these tasks, most of the success is due to the improved control algorithms and vehicle specifications of quadrotors [6]. How quadrotors work is described in Figure 1.1 basically.

With the developing technology, the installation of these vehicles is very simple and their dimensions have become lighter than 1 kg, shorter than 10 cm [8] . In spite of these improvements, performance at the desired level in the intended application is largely based on the developed control algorithm. Due to its complex and under-actuated dynamic model, control algorithm design for quadrotors involves significant difficulties [9]. The mathematical modeling of the basic dynamics is the starting point of the work on this subject. There are more realistic mathematical models which have been created by adding more aerodynamic effects and dynamics [10–13]. Various inner loop control methods have been used to keep these vehicles in balance and to make certain special maneuvers by taking measurements from on-board sensors such as inertial measurement unit (IMU), pressure gauge, laser placed on the vehicle. Some of these methods include the PID controller [8, 14–16], the backstepping method [17, 18], the neural network based control method [19], nonlinear method [20], H infinity [21], saturation technique [22, 23]. These control algorithms are implemented so that a user gives commands instantaneously or specifies them previously to be performed by a quadrotor. However, a successful autonomous flight depends on not only a good inner loop controller, but also outer loop control algorithm.

The outer loop algorithms vary depending on the type of task, vehicle dynamics, sensor capacity, and task location characteristics. One of the most important areas of use of these tools is search and rescue examined under resource search and follow problems. For situations where the positions of both vehicle and source are precisely measured, a variety of algorithms for this task are available [24–28]. In addition, quadrotor-compliant image processing and tracking algorithms have been developed for situations where the position of the vehicle is measured but the image of the source is captured by the camera instead of measuring its position via GPS [29,30] . However, position measurement and useful image information may not always be possible. For

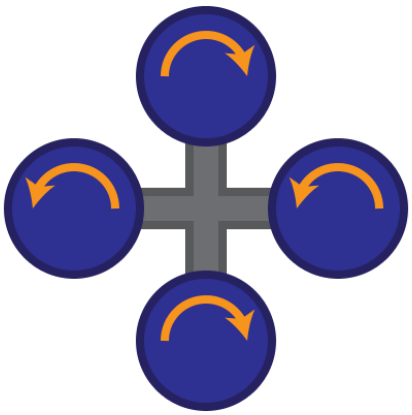

(a) Hovering or changing its altitude by applying same thrust to all the motors

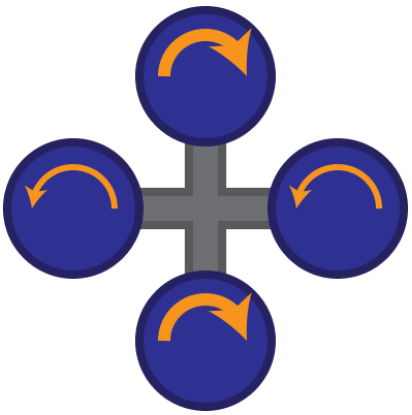

(b) Controlling its yaw angle by applying more thrust to the motors rotating in same direction

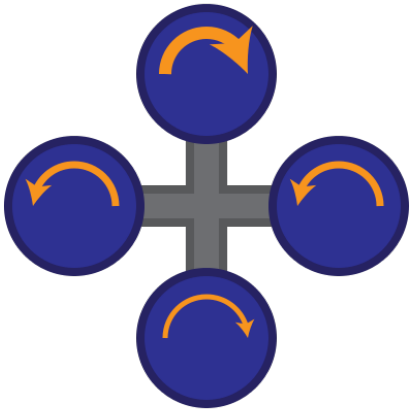

(c) Controlling its pitch or roll angle by applying more thrust to the rotor in opposite direction

Figure 1.1. Basic movements of a quadrotor

example, a vehicle can not perform the above tasks if it is in a place where the GPS signal is weak or not at all. In such cases, the deterministic [31,32] and the stochastic [33] extreme seeking algorithms which are real time optimization tools become useful. The schematic of the deterministic extremum seeking algorithm can be found in [31–34].

Extremum seeking control has been used in many systems, such as the control of chemical reactors [35,36], the reduction of fuel consumption of aircraft [37,38] and automobile applications [39], which are difficult to develop mathematical models for dynamic systems. The most important reason why the extremum seeking algorithm can be used for resource search and follow purposes is that the intensity of the signal emitted from the source decreases as the distance from the source increases and the most intense signal measurement occurs around the source. With this assumption in mind, this algorithm has been applied as a resource discovery-lookup algorithm in nonhonomic nonlinear dynamical vehicles [40–42]. The algorithm ensures that vehicles turn to the direction of a signal source by being oscillated on the target plane. In the studies made for the two dimensions, the linear velocity of the vehicle is kept constant and the orientation is changed by changing the angular velocity [40,41,43]. By adding the linear velocity to the extremum seeking algorithm, it was provided with a narrower maneuvering approach [44].

1.2. Purpose

The personal usage of quadrotors is becoming available as a result of accurate analysis of the measurements obtained by the on-board sensors. As stated in Section 1.1, different control methods such as PID [8, 14–16], backstepping [17, 18], neural network [19], nonlinear method [20], H infinity [21], saturated control [22, 23] have been used. The most widely used ones are PID controllers. The biggest advantage of PID controllers is that their application is very simple, but one of their biggest problems is the risk of instability when the environmental conditions or the physical properties of the vehicle change. The control parameters have to be set again by trial and error method depending on vehicle or its usage. One of the robust control techniques, H infinity control, is able to keep the vehicle in balance despite the uncertainties within a certain range, anticipating possible changes in vehicle dynamics. However, this controller can not prevent the vehicle from moving unevenly at a different equlibrium point or with unanticipated changes. Although neural network and similar input-output learning algorithms and system-balanced approaches have the potential to adapt to changing environments and structures, theoretically, stabilization is not always possible. Moreover, in every change of environment and physical condition, the renewal of the learning algorithm causes computation burden and time loss in the microprocessor on a quadrotor which is quite small in size. Adaptive control method is one of the most conveinent method to stabilize a system despite uncertainty in the system structure. There are some adaptive control method studies for quadrotors [17, 18] in the literature, however, they did not consider the uncertainty that might arise from the physical characteristics of the vehicle and the disturbance that could affect quadrotor dynamics together.

The first step of this work is designing an adaptive inner loop controller that can withstand periodic disturbances and vehicle variable parameters. This design, thanks to its adaptive feature, can be applied to quadrotors with different physical structure, it will not require any new adjustment during loading and unloading and it will be possible to stabilize the vehicle against periodical disturbances which may come from environmental conditions such as wind effect to make the desired maneuvers. Moreover,

small-angle approximation which is used to simplify the equations of Euler angles is not utilized so that the quadrotor has a better maneuverability.

Resource locating and search algorithms for situations where GPS is not possible have been applied to vehicles with one degree freedom [40, 41, 43]. A similar approach has been applied to 2D space point mass [44] and autonomous underwater vehicle [42] in 3D. The purpose of these studies is to direct the vehicle towards the center of any kind of source where the signal is most intense,assuming that the signal of reduced intensity is measured by the sensor on the vehicle as it moves away from the source. The studies are accomplished for vehicles with basic dynamics. The algorithm has not been implemented on quadrotor.

The second step of this work is implementing extremum seeking algorithm to a quadrotor so that the quadrotor can find a light source around itself. In [45], the task is accomplished by creating a gradient field of map via the information obtained from the sensors measuring the relative signal strength and the respective positions of cooperative quadrotors. This work is different in that no position sensor and no more than one quadrotor are needed to localize the source. In [46], a quadrotor has to turn along the vertical axis continuously and sense the signal value of the corresponding yaw angle. The advantage of this design is that instead of rotating the quadrotor continuously, the servo motor arm onto which the sensor attached rotates to seek the source which results in more stable flight.

2. SYSTEM MODELING

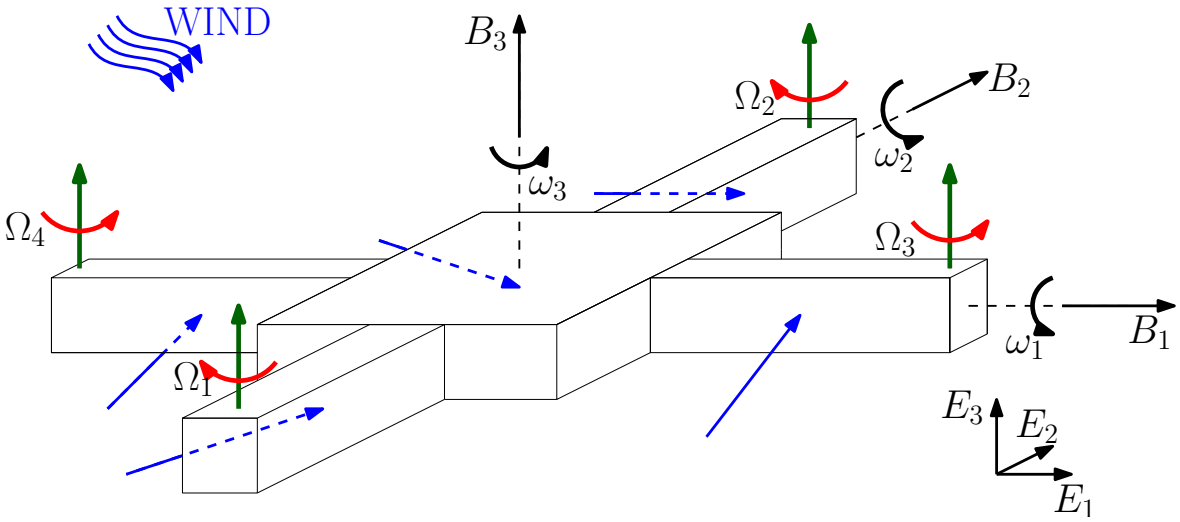

Figure 2.1. Scheme of quadrotor. The blue lines represents the wind velocity vector at 5 nodes defined on the quadrotor.

The scheme of a quadrotor under consideration in this thesis is demonstrated in Figure 2.1. It has four rotors which each of them generates thrust force and moment along B_3 as shown in Figure 2.1. The pair of motors (1,2) rotate in clockwise direction while the other pair (3,4) rotates in counter-clockwise direction to avoid yaw drift. To change the yaw angle, one can increase the angular velocity of a pair with respect to the angular velocity of the other pair. The vertical position of a quadrotor changes by actuating thrust forces of the motors equally. A quadrotor can achieve the forward (backward) motion by lowering the angular velocity of motor 3(4) and increasing the angular velocity of motor 4(3). Finally, right(left) side motion is accomplished by lowering the angular velocity of motor 1(2) and increasing the angular velocity of motor 2(1).

2.1. Kinematic Model

Let $B = B_1, B_2, B_3$ be the body fixed frame BFF and $E = E_1, E_2, E_3$ be the earth fixed frame EFF as presented in Figure 2.1. The rotation matrix, $R(\phi, \theta, \psi) \in \mathbb{R}^3$, from

EFF to BFF is given by;

$$R = \begin{bmatrix} c_\theta c_\psi & c_\theta s_\psi & -s_\theta \\ s_\phi s_\theta c_\psi - c_\phi s_\psi & s_\phi s_\theta s_\psi + c_\phi c_\psi & s_\phi c_\theta \\ c_\phi s_\theta c_\psi + s_\phi s_\psi & c_\phi s_\theta s_\psi - s_\phi c_\psi & c_\phi c_\theta \end{bmatrix}, \tag{2.1}$$

where ϕ, θ, ψ are the Euler angles representing the orientation of quadrotor. $c_()$, $s_()$ and $t_()$ represent $cos()$, $sin()$ and $tan()$, respectively.

Defining $\omega_1, \omega_2, \omega_3$ as the angular velocities with respect to BFF, the rotational kinematic equation is given by

$$\begin{bmatrix} \dot{\phi} \\ \dot{\theta} \\ \dot{\psi} \end{bmatrix} = W \begin{bmatrix} \omega_1 \\ \omega_2 \\ \omega_3 \end{bmatrix} \tag{2.2}$$

where W is the 3x3 transfer matrix,

$$W = \begin{bmatrix} 1 & s_\phi t_\theta & c_\phi t_\theta \\ 0 & c_\phi & -s_\phi \\ 0 & s_\phi / c_\theta & c_\phi / c_\theta \end{bmatrix}. \tag{2.3}$$

In general, the small angle approximation is used to equalizing the matrix W to an identity matrix which makes the dynamic equation of Euler Angles be same as the dynamics of the angular velocity with respect to BFF. However, in this adaptive control design, this approximation is not used so that quadrotor has better maneuverability.

2.2. Equations of Motions

The model developed in this thesis assumes the following;

- The structure is supposed rigid.
- The structure is supposed symmetrical.
- The center of gravity of quadrotor coincides with the origin of BFF.
- Thrust and drag of each rotor are proportional to the square of propeller's speed.
- The angular speed of rotor is proportional to the input voltage of rotor.

Hence, the dynamic equations of angular velocities with respect to BFF and the position with respect to EFF are given by

$$\dot{\omega}_1 = p_2\Omega_2^2 - p_1\Omega_1^2 + \omega_2\omega_3\tau_1 + \nu_1, \tag{2.4}$$

$$\dot{\omega}_2 = p_4\Omega_4^2 - p_3\Omega_3^2 + \omega_1\omega_3\tau_2 + \nu_2, \tag{2.5}$$

$$\dot{\omega}_3 = q_1\Omega_1^2 + q_2\Omega_2^2 - q_3\Omega_3^2 - q_4\Omega_4^2 + \omega_1\omega_2\tau_3 + \nu_3, \tag{2.6}$$

$$\ddot{z} = c_\phi c_\theta \sum_{i=1}^{4} r_i\Omega_i^2 - g + \nu_4, \tag{2.7}$$

$$\ddot{x} = (c_\phi s_\theta c_\psi + s_\phi s_\psi) \sum_{i=1}^{4} r_i\Omega_i^2 + \nu_x, \tag{2.8}$$

$$\ddot{y} = (c_\phi s_\theta s_\psi - s_\phi c_\psi) \sum_{i=1}^{4} r_i\Omega_i^2 + \nu_y, \tag{2.9}$$

where Ω_1, Ω_2, Ω_3, Ω_4 are the angular speed of the motors' shafts, τ_1, τ_2, τ_3 are $\frac{J_{22}-J_{33}}{J_{11}}$, $\frac{J_{33}-J_{11}}{J_{22}}$, $\frac{J_{11}-J_{22}}{J_{33}}$ respectively with the principal moments of inertia J_{11}, J_{22}, J_{33} with respect to BFF, ν_1, ν_2, ν_3, ν_4, ν_x and ν_y are the wind disturbances which are described in Section 2.3, $\ddot{x}$, $\ddot{y}$, $\ddot{z}$ are the acceleration of the quadrotor along E_1, E_2, E_3, g is the gravity, $p_{i_1} = \frac{b_{i_1} l_{i_1}}{J_{11}}$, $p_{i_2} = \frac{b_{i_2} l_{i_2}}{J_{22}}$, $q_i = \frac{d_i}{J_{zz}}$, $r_i = \frac{b_i}{m}$ with b_i, d_i, l_i representing the thrust, the drag factors of the propellers and the lengths of arms of quadrotor respectively. By taking the derivation of (2.2) with respect to time which is given by;

$$\begin{bmatrix} \ddot{\phi} \\ \ddot{\theta} \\ \ddot{\psi} \end{bmatrix} = \dot{W} \begin{bmatrix} \omega_1 \\ \omega_2 \\ \omega_3 \end{bmatrix} + W \begin{bmatrix} \dot{\omega}_1 \\ \dot{\omega}_2 \\ \dot{\omega}_3 \end{bmatrix}, \tag{2.10}$$

the dynamic equations of Euler angles is written as;

$$\ddot{\phi} = \dot{\omega}_1 + s_\phi t_\theta \dot{\omega}_2 + c_\phi t_\theta \dot{\omega}_3 + \kappa_1 \tag{2.11}$$

$$\ddot{\theta} = c_\phi \dot{\omega}_2 - s_\phi \dot{\omega}_3 + \kappa_2 \tag{2.12}$$

$$\ddot{\psi} = \frac{s_\phi}{c_\theta} \dot{\omega}_2 + \frac{c_\phi}{c_\theta} \dot{\omega}_3 + \kappa_3 \tag{2.13}$$

where

$$\begin{bmatrix} \kappa_1 \\ \kappa_2 \\ \kappa_3 \end{bmatrix} = \dot{W} \begin{bmatrix} \omega_1 \\ \omega_2 \\ \omega_3 \end{bmatrix} \tag{2.14}$$

2.3. Wind Disturbance

To simulate the wind disturbance on a quadrotor, a wind vector field is created as a function of time and the position of a point with respect to EFF by using Dryden gust model in [11].

The calculation is done to find the wind velocity with respect to BFF at 5 nodes which 4 of them are at the center of quadrotor's arms and the fifth one is at the center of quadrotor as seen in Figure 2.1. By using the basic formula of wind force which is given by

$$U_{wind} = \frac{1}{2} \rho A C_D V_{wind}^2 \tag{2.15}$$

where U_{wind} is the drag force of wind, ρ is the air density, A is the area subjected to the wind, C_D is the drag coefficient, V_{wind} is the relative velocity of wind with respect to the quadrotor, the wind forces and the moment of these forces on each point are calculated. Summing the forces and the moments applied to each node up, the wind

disturbances are obtained as

$$\begin{bmatrix} \nu_1 \\ \nu_2 \\ \nu_3 \\ \nu_x \\ \nu_y \\ \nu_z \end{bmatrix} = \begin{bmatrix} \sum_{i_1=1}^{5} M_{wind,i} \\ R \sum_{i_1=1}^{5} U_{wind,i} \end{bmatrix} \tag{2.16}$$

where $M_{wind,i}$ is the moment disturbance of wind at i$^{\text{th}}$ node. The detailed calculations for the wind disturbances are given in Appendix A.

3. ADAPTIVE CONTROLLER DESIGN AND RESULTS

3.1. Wind Disturbance Observer

Before starting explaning the observer design, it should be stated that (2.16) is used in simulation to test the performance of controller in more realistic environment. Morever, the observer is designed for all wind disturbances except ν_x and ν_y due to the fact that the controller is not designed to control the position of quadrotors in the horizantal plane. For the sake of the design of a controller, it is assumed that the wind disturbances are given by,

$$\nu_1(t) = {}_0\sigma_1 + \sum_{s=1}^{n} {}_s\sigma_1 sin({}_s\alpha_1 t + {}_s\Phi_1) \tag{3.1}$$

$$\nu_2(t) = {}_0\sigma_2 + \sum_{s=1}^{n} {}_s\sigma_2 sin({}_s\alpha_2 t + {}_s\Phi_2) \tag{3.2}$$

$$\nu_3(t) = {}_0\sigma_3 + \sum_{s=1}^{n} {}_s\sigma_3 sin({}_s\alpha_3 t + {}_s\Phi_3) \tag{3.3}$$

$$\nu_4(t) = {}_0\sigma_4 + \sum_{s=1}^{n} {}_s\sigma_4 sin({}_s\alpha_4 t + {}_s\Phi_4) \tag{3.4}$$

$$\tag{3.5}$$

where the amplitude, ${}_s\sigma_1$, ${}_s\sigma_2$, ${}_s\sigma_3$, ${}_s\sigma_4$, the frequency, ${}_s\alpha_1$, ${}_s\alpha_2$, ${}_s\alpha_3$, ${}_s\alpha_4$, the phase ${}_s\Phi_1$, ${}_s\Phi_2$, ${}_s\Phi_3$, ${}_s\Phi_4$ and the constant disturbance, ${}_0\sigma_1$, ${}_0\sigma_2$, ${}_0\sigma_3$, ${}_0\sigma_4$, are unknown. The number of maximum distinct frequencies n is known. In the next section, an observer design for the wind disturbance is introduced.

Wind disturbances given in (3.1)–(3.4) can be represented as outputs of linear exosystems,

$$\dot{Z}_1(t) = S_1 Z_1(t), \quad \nu_1(t) = h_1^T Z_1(t), \tag{3.6}$$

$$\dot{Z}_2(t) = S_2 Z_2(t), \quad \nu_2(t) = h_2^T Z_2(t), \tag{3.7}$$

$$\dot{Z}_3(t) = S_3 Z_3(t), \quad \nu_3(t) = h_3^T Z_3(t), \tag{3.8}$$

$$\dot{Z}_4(t) = S_4 Z_4(t), \quad \nu_4(t) = h_4^T Z_4(t), \tag{3.9}$$

where $Z_1(t)$, $Z_2(t)$, $Z_3(t)$, $Z_4(t) \in \mathbb{R}^{2n+1}$, and the matrices S_1, S_2, S_3, S_4 depend on the unknown frequencies of the wind disturbances ν_1, ν_2, ν_3, ν_4, while the uncertainties of the amplitudes and the phases are related to the unknown initial condition of (3.6)–(3.9).

The wind disturbances are parametrized by following [47]. Let $G \in \mathbb{R}^{(2n+1)\times(2n+1)}$ be a Hurwitz matrix with distinct eigenvalues and let (G, L) be a controllable pair. Since (h_1^T, S_1), (h_2^T, S_2), (h_3^T, S_3), $(h_4 i^T, S_4)$ are observable and the spectra of S_1, S_2, S_3, S_4 and G_1, G_2, G_3, G_4 are disjoint, the unique solutions M_1, M_2, M_3, M_4, $\in \mathbb{R}^{(2n+1)\times(2n+1)}$ of the Sylvester equations,

$$M_1 S_1 - G M_1 = L h_1^T, \tag{3.10}$$

$$M_2 S_2 - G M_2 = L h_2^T, \tag{3.11}$$

$$M_3 S_3 - G M_3 = L h_3^T, \tag{3.12}$$

$$M_4 S_4 - G M_4 = L h_4^T, \tag{3.13}$$

are invertible [48]. By applying a state transformation with the matrices $\chi_1 = M_1 Z_1$, $\chi_2 = M_2 Z_2$, $\chi_3 = M_3 Z_3$, $\chi_4 = M_4 Z_4$ equations take form of,

$$\dot{\chi}_1(t) = G\chi_1(t) + L\nu_1(t), \tag{3.14}$$

$$\dot{\chi}_2(t) = G\chi_2(t) + L\nu_2(t), \tag{3.15}$$

$$\dot{\chi}_3(t) = G\chi_3(t) + L\nu_3(t), \tag{3.16}$$

$$\dot{\chi}_4(t) = G\chi_4(t) + L\nu_4(t), \tag{3.17}$$

$$\nu_1(t) = \beta_1^T \chi_1(t), \tag{3.18}$$

$$\nu_2(t) = \beta_2^T \chi_2(t), \tag{3.19}$$

$$\nu_3(t) = \beta_3^T \chi_3(t), \tag{3.20}$$

$$\nu_4(t) = \beta_4^T \chi_4(t), \tag{3.21}$$

where $\beta_1^T = h_1^T M_1^{-1}$, $\beta_2^T = h_2^T M_2^{-1}$, $\beta_3^T = h_3^T M_3^{-1}$, $\beta_4^T = h_4^T M_4^{-1} \in \mathbb{R}^{(2n+1)}$.

Unknown disturbance terms $\nu_1(t)$, $\nu_2(t)$, $\nu_3(t)$, $\nu_4(t)$ are represented as product of two unknown terms in equation (3.18)–(3.21), namely unknown constant vectors β_1^T, β_2^T, β_3^T, β_4^T and unknown time dependent vectors $\chi_1(t)$, $\chi_2(t)$, $\chi_3(t)$, $\chi_4(t)$. In order to be able to estimate $\chi_1(t)$, $\chi_2(t)$, $\chi_3(t)$, $\chi_4(t)$, conceptual observers are designed. The following lemma establishes the properties of the observer.

Lemma 3.1. *The inaccessible disturbances $\nu_1(t)$, $\nu_2(t)$, $\nu_3(t)$ and $\nu_4(t)$ can be represented in the form*

$$\nu_1(t) = \beta_1^T \delta_1 + \beta_1^T \xi_1 + \beta_{p_2}^T \eta_{p_2} + \beta_{p_1}^T \eta_{p_1} + \beta_{\tau_1}^T \eta_{\tau_1}, \tag{3.22}$$

$$\nu_2(t) = \beta_2^T \delta_2 + \beta_2^T \xi_2 + \beta_{p_4}^T \eta_{p_4} + \beta_{p_3}^T \eta_{p_3} + \beta_{\tau_2}^T \eta_{\tau_2}, \tag{3.23}$$

$$\nu_3(t) = \beta_3^T \delta_3 + \beta_3^T \xi_3 + \beta_{q_1}^T \eta_{p_1} + \beta_{q_2}^T \eta_{p_2} + \beta_{q_3}^T \eta_{p_3} + \beta_{q_4}^T \eta_{p_4} + \beta_{\tau_3}^T \eta_{\tau_3}, \tag{3.24}$$

$$\nu_4(t) = \beta_4^T \delta_4 + \beta_4^T \xi_4 + \beta_{r_1}^T \eta_{p_1} + \beta_{r_2}^T \eta_{p_2} + \beta_{r_3}^T \eta_{p_3} + \beta_{r_4}^T \eta_{p_4}, \tag{3.25}$$

where $\beta_{p_1}^T = -\beta_1^T p_1$, $\beta_{p_2}^T = \beta_1^T p_2$, $\beta_{p_3}^T = -\beta_2^T p_3$, $\beta_{p_4}^T = \beta_2^T p_4$, $\beta_{q_1}^T = \beta_3^T q_1$, $\beta_{q_2}^T = \beta_3^T q_2$, $\beta_{q_3}^T = -\beta_3^T q_3$, $\beta_{q_4}^T = -\beta_3^T q_4$, $\beta_{r_i}^T = \beta_4^T r_i$, $\beta_{\tau_j}^T = \beta_j^T \tau_j$ *with the following filters,*

$$\xi_1 = \eta_1 + L\omega_1, \tag{3.26}$$

$$\xi_2 = \eta_2 + L\omega_2, \tag{3.27}$$

$$\xi_3 = \eta_3 + L\omega_3, \tag{3.28}$$

$$\xi_4 = \eta_4 + L\dot{z}, \tag{3.29}$$

$$\dot{\eta}_1 = G\xi_1, \tag{3.30}$$

$$\dot{\eta}_2 = G\xi_2, \tag{3.31}$$

$$\dot{\eta}_3 = G\xi_3, \tag{3.32}$$

$$\dot{\eta}_4 = G\xi_4 + Lg, \tag{3.33}$$

$$\dot{\eta}_{\tau_1} = G\eta_{\tau_1} - L\omega_2\omega_3, \tag{3.34}$$

$$\dot{\eta}_{\tau_2} = G\eta_{\tau_2} - L\omega_1\omega_3, \tag{3.35}$$

$$\dot{\eta}_{\tau_3} = G\eta_{\tau_3} - L\omega_1\omega_2, \tag{3.36}$$

$$\dot{\eta}_{p_1} = G\eta_{p_1} - L\Omega_1^2 \tag{3.37}$$

$$\dot{\eta}_{p_2} = G\eta_{p_2} - L\Omega_2^2 \tag{3.38}$$

$$\dot{\eta}_{p_3} = G\eta_{p_3} - L\Omega_3^2 \tag{3.39}$$

$$\dot{\eta}_{p_4} = G\eta_{p_4} - L\Omega_4^2 \tag{3.40}$$

and the estimation errors δ_1, δ_2, δ_3 *and* $\delta_4 \in \mathbb{R}^{2q\times 1}$ *are defined as follows*

$$\delta_1 = \chi_1 - (\xi_1 + p_2\eta_{p_2} - p_1\eta_{p_1} + \tau_1\eta_{\tau_1}), \tag{3.41}$$

$$\delta_2 = \chi_2 - (\xi_2 + p_4\eta_{p_4} - p_3\eta_{p_3} + \tau_2\eta_{\tau_2}), \tag{3.42}$$

$$\delta_3 = \chi_3 - (\xi_3 + q_1\eta_{p_1} + q_2\eta_{p_2} - q_3\eta_{p_3} - q_4\eta_{p_4} + \tau_3\eta_{\tau_3}), \tag{3.43}$$

$$\delta_4 = \chi_4 - (\xi_4 + r_1\eta_{p_1} + r_2\eta_{p_2} + r_3\eta_{p_3} + r_4\eta_{p_4}), \tag{3.44}$$

and obeys the equations,

$$\dot{\delta}_1 = G\delta_1, \tag{3.45}$$

$$\dot{\delta}_2 = G\delta_2, \tag{3.46}$$

$$\dot{\delta}_3 = G\delta_3, \tag{3.47}$$

$$\dot{\delta}_4 = G\delta_4. \tag{3.48}$$

Proof. The equations (3.45)–(3.48) are obtained by differentiating (3.41)–(3.44) with respect to time and using (2.4)–(2.7), (3.14)–(3.17) and (3.26)–(3.40). Substitution of (3.41)–(3.44) into (3.18)–(3.21) yields (3.22)–(3.25). □

3.2. Controller Design

The error terms are defined between the Euler angles and desired trajectories as

$$\begin{bmatrix} e_1 \\ e_2 \\ e_3 \\ e_4 \end{bmatrix} = \begin{bmatrix} \phi - \phi_{des} \\ \dot{\phi} - \dot{\phi}_{des} \\ \theta - \theta_{des} \\ \dot{\theta} - \dot{\theta}_{des} \\ \psi - \psi_{des} \\ \dot{\psi} - \dot{\psi}_{des} \\ z - z_{des} \\ \dot{z} - \dot{z}_{des} \end{bmatrix}, \tag{3.49}$$

where e_1, e_2, e_3, $e_4 \in \mathbb{R}^2$. Considering (2.11)–(2.13) along with (2.4)–(2.6), the dynamics of error terms are obtained and they are complicated. Therefore, this part is given in Appendix B. As it is seen in (B.1)–(B.4), the effects of the control inputs, which are the angular speed of motors' shafts, are coupled.

The control laws for the angular speed of each motor's shaft are given by

$$\begin{bmatrix} \Omega_1^2 \\ \Omega_2^2 \\ \Omega_3^2 \\ \Omega_4^2 \end{bmatrix} = D^{-1} \begin{bmatrix} \Lambda_1 \\ \Lambda_2 \\ \Lambda_3 \\ \Lambda_4 \end{bmatrix}, \tag{3.50}$$

$$D = \begin{bmatrix} -\hat{p}_1 + c_\phi t_\theta \hat{q}_1 & \hat{p}_2 + c_\phi t_\theta \hat{q}_2 & -s_\phi t_\theta \hat{p}_3 - c_\phi t_\theta \hat{q}_3 & s_\phi t_\theta \hat{p}_4 - c_\phi t_\theta \hat{q}_4 \\ -s_\phi \hat{q}_1 & -s_\phi \hat{q}_2 & s_\phi \hat{q}_3 - c_\phi \hat{p}_3 & s_\phi \hat{q}_4 + c_\phi \hat{p}_4 \\ \frac{c_\phi}{c_\theta}\hat{q}_1 & \frac{c_\phi}{c_\theta}\hat{q}_2 & -\frac{c_\phi}{c_\theta}\hat{q}_3 - \frac{s_\phi}{c_\theta}\hat{p}_3 & -\frac{c_\phi}{c_\theta}\hat{q}_4 + \frac{s_\phi}{c_\theta}\hat{p}_4 \\ c_\phi c_\theta \hat{r}_1 & c_\phi c_\theta \hat{r}_2 & c_\phi c_\theta \hat{r}_3 & c_\phi c_\theta \hat{r}_4 \end{bmatrix} \tag{3.51}$$

$$\Lambda_1 = -\hat{\epsilon}_1 - s_\phi t_\theta \hat{\epsilon}_2 - c_\phi t_\theta \hat{\epsilon}_3 - \kappa_1 + \ddot{\phi}_{des} + K e_1 - \frac{e_1^T P B t_\theta^2}{\zeta} \tag{3.52}$$

$$\Lambda_2 = -c_\phi \hat{\epsilon}_2 + s_\phi \hat{\epsilon}_3 - \kappa_2 + \ddot{\theta}_{des} + K e_2 \tag{3.53}$$

$$\Lambda_3 = -\frac{s_\phi}{c_\theta}\hat{\epsilon}_2 - \frac{c_\phi}{c_\theta}\hat{\epsilon}_3 - \kappa_3 + \ddot{\psi}_{des} + K e_3 - \frac{e_3^T P B}{\zeta c_\theta^2} \tag{3.54}$$

$$\Lambda_4 = -\hat{\epsilon}_4 + g + \ddot{z}_{des} + K e_4 \tag{3.55}$$

$$\hat{\epsilon}_1 = \omega_2\omega_3\hat{\tau}_1 + \hat{\beta}_1^T\xi_1 + \hat{\beta}_{p_1}^T\eta_{p_1} + \hat{\beta}_{p_2}^T\eta_{p_2} + \hat{\beta}_{\tau_1}^T\eta_{\tau_1} \tag{3.56}$$

$$\hat{\epsilon}_2 = \omega_1\omega_3\hat{\tau}_2 + \hat{\beta}_2^T\xi_2 + \hat{\beta}_{p_3}^T\eta_{p_3} + \hat{\beta}_{p_4}^T\eta_{p_4} + \hat{\beta}_{\tau_2}^T\eta_{\tau_2} \tag{3.57}$$

$$\hat{\epsilon}_3 = \omega_1\omega_2\hat{\tau}_3 + \hat{\beta}_3^T\xi_3 + \hat{\beta}_{q_1}^T\eta_{p_1} + \hat{\beta}_{q_2}^T\eta_{p_2} + \hat{\beta}_{q_3}^T\eta_{p_3} + \hat{\beta}_{q_4}^T\eta_{p_4} + \hat{\beta}_{\tau_3}^T\eta_{\tau_3} \tag{3.58}$$

$$\hat{\epsilon}_4 = \hat{\beta}_4^T\xi_4 + \hat{\beta}_{r_1}^T\eta_{p_1} + \hat{\beta}_{r_2}^T\eta_{p_2} + \hat{\beta}_{r_3}^T\eta_{p_3} + \hat{\beta}_{r_4}^T\eta_{p_4} \tag{3.59}$$

where $\zeta > 0$, the control gain $K \in \mathbb{R}^{1\times 2}$ is chosen so that $(A + BK)$ is Hurwitz with $A = \begin{bmatrix} 0 & 1 \\ 0 & 0 \end{bmatrix}$ and $B = [0 \quad 1]^T$, the positive definite matrix P is solution of the equation,

$$(A + BK)^T P + P(A + BK) = -2\varphi I \tag{3.60}$$

and $\varphi > 0$.

The update laws are given by

$$\dot{\hat{p}}_1 = \begin{cases} 0, & \hat{p}_1 \leq p_{min} \quad \text{and} \quad \dot{\hat{p}}_1 < 0 \\ -\gamma_p \mu_1 \Omega_1^2, & \text{else if} \end{cases} \tag{3.61}$$

$$\dot{\hat{p}}_2 = \begin{cases} 0, & \hat{p}_2 \leq p_{min} \quad \text{and} \quad \dot{\hat{p}}_2 < 0 \\ \gamma_p \mu_1 \Omega_2^2, & \text{else if} \end{cases} \tag{3.62}$$

$$\dot{\hat{p}}_3 = \begin{cases} 0, & \hat{p}_3 \leq p_{min} \quad \text{and} \quad \dot{\hat{p}}_3 < 0 \\ -\gamma_p \mu_2 \Omega_3^2, & \text{else if} \end{cases} \tag{3.63}$$

$$\dot{\hat{p}}_4 = \begin{cases} 0, & \hat{p}_4 \leq p_{min} \quad \text{and} \quad \dot{\hat{p}}_4 < 0 \\ \gamma_p \mu_2 \Omega_4^2, & \text{else if} \end{cases} \tag{3.64}$$

$$\dot{\hat{q}}_1 = \begin{cases} 0, & \hat{q}_1 \leq q_{min} \quad \text{and} \quad \dot{\hat{q}}_1 < 0 \\ \gamma_q \mu_1 \Omega_1^2, & \text{else if} \end{cases} \tag{3.65}$$

$$\dot{\hat{q}}_2 = \begin{cases} 0, & \hat{q}_2 \leq q_{min} \quad \text{and} \quad \dot{\hat{q}}_2 < 0 \\ \gamma_q \mu_1 \Omega_2^2, & \text{else if} \end{cases} \tag{3.66}$$

$$\dot{\hat{q}}_3 = \begin{cases} 0, & \hat{q}_3 \leq q_{min} \quad \text{and} \quad \dot{\hat{q}}_3 < 0 \\ -\gamma_q \mu_2 \Omega_3^2, & \text{else if} \end{cases} \tag{3.67}$$

$$\dot{\hat{q}}_4 = \begin{cases} 0, & \hat{q}_4 \leq q_{min} \quad \text{and} \quad \dot{\hat{q}}_4 < 0 \\ -\gamma_q \mu_2 \Omega_4^2, & \text{else if} \end{cases} \tag{3.68}$$

$$\dot{\hat{r}}_1 = \begin{cases} 0, & \hat{r}_1 \leq r_{min} \quad \text{and} \quad \dot{\hat{r}}_1 < 0 \\ \gamma_r \mu_4 \Omega_1^2 c_\phi c_\theta, & \text{else} \end{cases} \tag{3.69}$$

$$\dot{\hat{r}}_2 = \begin{cases} 0, & \hat{r}_2 \leq r_{min} \quad \text{and} \quad \dot{\hat{r}}_2 < 0 \\ \gamma_r \mu_4 \Omega_2^2 c_\phi c_\theta, & \text{else} \end{cases} \tag{3.70}$$

$$\dot{\hat{r}}_3 = \begin{cases} 0, & \hat{r}_3 \leq r_{min} \quad \text{and} \quad \dot{\hat{r}}_3 < 0 \\ \gamma_r \mu_4 \Omega_3^2 c_\phi c_\theta, & \text{else} \end{cases} \tag{3.71}$$

$$\dot{\hat{r}}_4 = \begin{cases} 0, & \hat{r}_4 \leq r_{min} \quad \text{and} \quad \dot{\hat{r}}_4 < 0 \\ \gamma_r \mu_4 \Omega_4^2 c_\phi c_\theta, & \text{else} \end{cases} \tag{3.72}$$

$$\dot{\hat{\tau}}_1 = \gamma_\tau \mu_1 \omega_2 \omega_3, \tag{3.73}$$

$$\dot{\hat{\tau}}_2 = \gamma_\tau \mu_2 \omega_1 \omega_3, \tag{3.74}$$

$$\dot{\hat{\tau}}_3 = \gamma_\tau \mu_3 \omega_1 \omega_2, \tag{3.75}$$

$$\dot{\hat{\beta}}_{p_1} = \gamma_\beta \mu_1 \eta_{p_1}, \tag{3.76}$$

$$\dot{\hat{\beta}}_{p_2} = \gamma_\beta \mu_1 \eta_{p_2}, \tag{3.77}$$

$$\dot{\hat{\beta}}_{p_3} = \gamma_\beta \mu_2 \eta_{p_3}, \tag{3.78}$$

$$\dot{\hat{\beta}}_{p_4} = \gamma_\beta \mu_2 \eta_{p_4}, \tag{3.79}$$

$$\dot{\hat{\beta}}_1 = \gamma_\beta \mu_3 \eta_1, \tag{3.80}$$

$$\dot{\hat{\beta}}_2 = \gamma_\beta \mu_3 \eta_2, \tag{3.81}$$

$$\dot{\hat{\beta}}_3 = \gamma_\beta \mu_3 \eta_3, \tag{3.82}$$

$$\dot{\hat{\beta}}_4 = \gamma_\beta \mu_3 \eta_4, \tag{3.83}$$

$$\dot{\hat{\beta}}_{\lambda_1} = \gamma_\beta \mu_1 \eta_{\lambda_1}, \tag{3.84}$$

$$\dot{\hat{\beta}}_{\lambda_2} = \gamma_\beta \mu_2 \eta_{\lambda_2}, \tag{3.85}$$

$$\dot{\hat{\beta}}_{\lambda_3} = \gamma_\beta \mu_3 \eta_{\lambda_3}, \tag{3.86}$$

$$\dot{\hat{\beta}}_{r_1} = \gamma_\beta \mu_4 \eta_1, \tag{3.87}$$

$$\dot{\hat{\beta}}_{r_2} = \gamma_\beta \mu_4 \eta_2, \tag{3.88}$$

$$\dot{\hat{\beta}}_{r_3} = \gamma_\beta \mu_4 \eta_3, \tag{3.89}$$

$$\dot{\hat{\beta}}_{r_4} = \gamma_\beta \mu_4 \eta_4, \tag{3.90}$$

$$\dot{\hat{\beta}}_1 = \gamma_\beta \mu_1 \xi_1, \tag{3.91}$$

$$\dot{\hat{\beta}}_2 = \gamma_\beta \mu_2 \xi_2, \tag{3.92}$$

$$\dot{\hat{\beta}}_3 = \gamma_\beta \mu_3 \xi_3, \tag{3.93}$$

$$\dot{\hat{\beta}}_4 = \gamma_\beta \mu_4 \xi_4, \tag{3.94}$$

where $\gamma_p, \gamma_q, \gamma_r, \gamma_\tau, \gamma_\beta > 0$ are update gains and

$$\mu_1 = e_1^T PB, \tag{3.95}$$

$$\mu_2 = e_1^T PBs_\phi t_\theta + e_2^T PBc_\phi + e_3^T PB\frac{s_\phi}{c_\theta}, \tag{3.96}$$

$$\mu_3 = e_1^T PBc_\phi t_\theta - e_2^T PBs_\phi + e_3^T PB\frac{c_\phi}{c_\theta}, \tag{3.97}$$

$$\mu_4 = e_4^T PB. \tag{3.98}$$

Assumption 1. *$p_i > p_{min} > 0$, $q_i > q_{min} > 0$ and $r_i > r_{min} > 0$ where p_{min}, q_{min} and r_{min} are known.*

Assumption 2. *The roll angle and the pitch angle satisfies $-\frac{\pi}{2} < \phi(t) < \frac{\pi}{2}$ and $-\frac{\pi}{2} < \theta(t) < \frac{\pi}{2}$*

Projection operators are applied as seen in (3.61)–(3.72) to ensure the determinant of D which is given by

$$\begin{aligned}\det(D) =& c_\phi(\hat{p}_2\hat{p}_3\hat{q}_4\hat{r}_1 + \hat{p}_2\hat{p}_4\hat{q}_3\hat{r}_1 + \hat{p}_1\hat{p}_3\hat{q}_4\hat{r}_2 + \hat{p}_1\hat{p}_4\hat{q}_3\hat{r}_2 + \hat{p}_1\hat{p}_4\hat{q}_2\hat{r}_3 + \hat{p}_2\hat{p}_4\hat{q}_1\hat{r}_3 \\ &+ \hat{p}_1\hat{p}_3\hat{q}_2\hat{r}_4 + \hat{p}_2\hat{p}_3\hat{q}_1\hat{r}_4),\end{aligned} \tag{3.99}$$

is not equal to zero by using Assumption 1–2.

Theorem 3.2. *Consider the closed-loop system consisting of the plant* (2.7) *and* (2.11) – (2.13) *forced by the unknown sinusoidal disturbances* (3.1)–(3.4)*, the disturbance observer* (3.26) – (3.40) *and the adaptive controller* (3.50) *with the update laws* (3.61) – (3.94)*. For all initial conditions such that $\hat{p}_1(0)$, $\hat{p}_2(0)$ $\hat{p}_3(0)$, $\hat{p}_4(0) > p_{min}$, $\hat{q}_1(0)$, $\hat{q}_2(0)$ $\hat{q}_3(0)$, $\hat{q}_4(0) > q_{min}$, and $\hat{r}_1(0)$, $\hat{r}_2(0)$ $\hat{r}_3(0)$, $\hat{r}_4(0) > r_{min}$, under Assumptions 1 – 2, all closed loop signals are bounded and the signals $e_1(t)$, $e_2(t)$, $e_3(t)$, $e_4(t)$, which are given in* (3.49) *, and $\delta_1(t)$,$\delta_2(t)$,$\delta_3(t)$,$\delta_4(t)$ converge to zero as $t \to \infty$. Specifically, perfect attitude and altitude reference tracking is achieved.*

3.3. Stability Proof

The closed loop error system is given by

$$\begin{aligned}
\dot{e}_1 =&(A+BK)e_1 + B\bigg(-\tilde{p}_1\Omega_1^2 + \tilde{p}_2\Omega_2^2 + \bar{\epsilon}_1 + s_\phi t_\theta(-\tilde{p}_3\Omega_3^2 + \tilde{p}_4\Omega_4^2 + \bar{\epsilon}_2) \\
&+ c_\phi t_\theta(\tilde{q}_1\Omega_1^2 + \tilde{q}_2\Omega_2^2 - \tilde{q}_3\Omega_3^2 - \tilde{q}_4\Omega_4^2 + \bar{\epsilon}_3) - \frac{e_1^T PBt_\theta^2}{\zeta}\bigg) \qquad (3.100)\\
\dot{e}_2 =&(A+BK)e_2 + B\bigg(c_\phi(-\tilde{p}_3\Omega_3^2 + \tilde{p}_4\Omega_4^2 + \bar{\epsilon}_2) - s_\phi(\tilde{q}_1\Omega_1^2 + \tilde{q}_2\Omega_2^2 - \tilde{q}_3\Omega_3^2 \\
&- \tilde{q}_4\Omega_4^2 + \bar{\epsilon}_3)\bigg) \qquad (3.101)\\
\dot{e}_3 =&(A+BK)e_3 + B\bigg(\frac{s_\phi}{c_\theta}(-\tilde{p}_3\Omega_3^2 + \tilde{p}_4\Omega_4^2 + \bar{\epsilon}_2) + \frac{c_\phi}{c_\theta}(\tilde{q}_1\Omega_1^2 + \tilde{q}_2\Omega_2^2 - \tilde{q}_3\Omega_3^2 \\
&- \tilde{q}_4\Omega_4^2 + \bar{\epsilon}_3) - \frac{e_3^T PB}{\zeta c_\theta^2}\bigg) \qquad (3.102)\\
\dot{e}_4 =&(A+BK)e_4 + B\bigg(c_\phi c_\theta(\tilde{r}_1\Omega_1^2 + \tilde{r}_2\Omega_2^2 + \tilde{r}_3\Omega_3^2 + \tilde{r}_4\Omega_4^2) + \bar{\epsilon}_4\bigg) \qquad (3.103)
\end{aligned}$$

where

$$\begin{aligned}
\bar{\epsilon}_1 =&\omega_2\omega_3\tilde{\tau}_1 + \tilde{\beta}_1^T\xi_1 + \tilde{\beta}_{p_1}^T\eta_{p_1} + \tilde{\beta}_{p_2}^T\eta_{p_2} + \tilde{\beta}_{\tau_1}^T\eta_{\tau_1} + \beta_1^T\delta_1 \qquad (3.104)\\
\bar{\epsilon}_2 =&\omega_1\omega_3\tilde{\tau}_2 + \tilde{\beta}_2^T\xi_2 + \tilde{\beta}_{p_3}^T\eta_{p_3} + \tilde{\beta}_{p_4}^T\eta_{p_4} + \tilde{\beta}_{\tau_2}^T\eta_{\tau_2} + \beta_2^T\delta_2 \qquad (3.105)\\
\bar{\epsilon}_3 =&\omega_1\omega_2\tilde{\tau}_3 + \tilde{\beta}_3^T\xi_3 + \tilde{\beta}_{q_1}^T\eta_{p_1} + \tilde{\beta}_{q_2}^T\eta_{p_2} + \tilde{\beta}_{q_3}^T\eta_{p_3} + \tilde{\beta}_{q_4}^T\eta_{p_4} + \tilde{\beta}_{\tau_3}^T\eta_{\tau_3} + \beta_3^T\delta_3 \qquad (3.106)\\
\bar{\epsilon}_4 =&\tilde{\beta}_4^T\xi_4 + \tilde{\beta}_{r_1}^T\eta_{p_1} + \tilde{\beta}_{r_2}^T\eta_{p_2} + \tilde{\beta}_{r_3}^T\eta_{p_3} + \tilde{\beta}_{r_4}^T\eta_{p_4} + \beta_4^T\delta_4 \qquad (3.107)
\end{aligned}$$

The symbol " ˜ " is used to denote the error between an actual parameter and its estimation. For instance, $\tilde{p} = p - \hat{p}$ where p is an unknown constant, $\hat{p}$ is its estimation and $\tilde{p}$ is the error between the unknown constant and its estimation.

In this section, the stability of the equilibrium of the closed loop system is established with the use of the following Lyapunov function,

$$V = \frac{1}{2}\Bigg(\sum_{i=1}^{4} e_i^T P e_i + \sum_{i=1}^{4} \frac{\tilde{p}_i^2}{\gamma_p} + \sum_{i=1}^{4} \frac{\tilde{q}_i^2}{\gamma_q} + \sum_{j=1}^{3} \frac{\tilde{\tau}_j^2}{\gamma_\tau} + \sum_{i=1}^{4} \frac{\tilde{r}_i^2}{\gamma_r} + \sum_{i=1}^{4} \frac{\tilde{\beta}_{p_i}^T \tilde{\beta}_{p_i}}{\gamma_\beta} + \sum_{i=1}^{4} \frac{\tilde{\beta}_{q_i}^T \tilde{\beta}_{q_i}}{\gamma_\beta} + \sum_{j=1}^{3} \frac{\tilde{\beta}_{\tau_j}^T \tilde{\beta}_{\tau_j}}{\gamma_\beta} + \sum_{i=1}^{4} \frac{\tilde{\beta}_{r_i}^T \tilde{\beta}_{r_i}}{\gamma_\beta} + \sum_{i=1}^{4} \frac{\tilde{\beta}_i^T \tilde{\beta}_i}{\gamma_\beta} + \sum_{i=1}^{4} \delta_i^T P_{\delta_i} \delta_i \Bigg), \tag{3.108}$$

where the positive definite matrices $P_{\delta_1},\ P_{\delta_2},\ P_{\delta_3},\ P_{\delta_4}$, are solutions of the matrix equations,

$$G^T P_{\delta_1} + P_{\delta_1} G = -2\varphi_{\delta_1} I, \tag{3.109}$$

$$G^T P_{\delta_2} + P_{\delta_2} G = -2\varphi_{\delta_2} I, \tag{3.110}$$

$$G^T P_{\delta_3} + P_{\delta_3} G = -2\varphi_{\delta_3} I, \tag{3.111}$$

$$G^T P_{\delta_4} + P_{\delta_4} G = -2\varphi_{\delta_4} I, \tag{3.112}$$

with

$$\varphi_{\delta_1} = \frac{\lambda_{max}(\beta_1 B^T P P B \beta_1^T)}{2\varphi} + 1, \tag{3.113}$$

$$\varphi_{\delta_2} = \frac{\lambda_{max}(\beta_2 B^T P P B \beta_2^T)}{\varphi} + \lambda_{max}(\beta_2 \beta_2^T)\zeta + 1, \tag{3.114}$$

$$\varphi_{\delta_3} = \frac{\lambda_{max}(\beta_3 B^T P P B \beta_3^T)}{\varphi} + \lambda_{max}(\beta_3 \beta_3^T)\zeta + 1, \tag{3.115}$$

$$\varphi_{\delta_4} = \frac{\lambda_{max}(\beta_4 B^T P P B \beta_4^T)}{2\varphi} + 1. \tag{3.116}$$

Taking time derivative of $V(t)$, in view of (3.61)-(3.94), using Young's inequality for the cross terms, it is obtained that

$$\dot{V} \leq -\frac{\gamma}{2} e_1^T e_1 - \frac{\gamma}{2} e_2^T e_2 - \gamma e_3^T e_3 - \frac{\gamma}{2} e_4^T e_4 - \sum_{i=1}^{4} \delta_i^T \delta_i \tag{3.117}$$

and it is concluded that

$$V(t) \leq V(0) \tag{3.118}$$

Defining

$$\Upsilon = \left[e_i, \delta_i, \tilde{p}_i, \tilde{q}_i, \tilde{\tau}_j, \tilde{r}_i, \tilde{\beta}_{p_i}, \tilde{\beta}_{q_i}, \tilde{\beta}_{\tau_j}, \tilde{\beta}_{r_i}, \tilde{\beta}_i \right]^T, \tag{3.119}$$

and using (3.108) and (3.118), it is obtained that

$$|\Upsilon|^2 \leq M_1 |\Upsilon(0)|, \tag{3.120}$$

for some M_1>0. From (3.120), it is obtained the uniform boundness of $|e_1(t)|$, $|e_2(t)|$, $|e_3(t)|$, $|e_4(t)|$, $|\delta_1(t)|$, $|\delta_2(t)|$, $|\delta_3(t)|$, $|\delta_4(t)|$, $|\tilde{p}_1(t)|$, $|\tilde{p}_2(t)|$, $|\tilde{p}_3(t)|$, $|\tilde{p}_4(t)|$, $|\tilde{q}_1(t)|$, $|\tilde{q}_2(t)|$, $|\tilde{q}_3(t)|$, $|\tilde{q}_4(t)|$, $|\tilde{r}_1(t)|$, $|\tilde{r}_2(t)|$, $|\tilde{r}_3(t)|$, $|\tilde{r}_4(t)|$, $|\tilde{\tau}_1(t)|$, $|\tilde{\tau}_2(t)|$, $|\tilde{\tau}_3(t)|$, $|\tilde{\beta}_1(t)|$, $|\tilde{\beta}_2(t)|$, $|\tilde{\beta}_3(t)|$, $|\tilde{\beta}_4(t)|$, $|\tilde{\beta}_{p_1}(t)|$, $|\tilde{\beta}_{p_2}(t)|$, $|\tilde{\beta}_{p_3}(t)|$, $|\tilde{\beta}_{p_4}(t)|$, $|\tilde{\beta}_{q_1}(t)|$, $|\tilde{\beta}_{q_2}(t)|$, $|\tilde{\beta}_{q_3}(t)|$, $|\tilde{\beta}_{q_4}(t)|$, $|\tilde{\beta}_{r_1}(t)|$, $|\tilde{\beta}_{r_2}(t)|$, $|\tilde{\beta}_{r_3}(t)|$, $|\tilde{\beta}_{r_4}(t)|$, $|\tilde{\beta}_{\tau_1}(t)|$, $|\tilde{\beta}_{\tau_2}(t)|$, $|\tilde{\beta}_{\tau_3}(t)|$. As the desired trajectories $|\phi_{des}(t)|$, $|\dot{\phi}_{des}(t)|$,$|\theta_{des}(t)|$,$|\dot{\theta}_{des}(t)|$, $|\psi_{des}(t)|$, $|\dot{\psi}_{des}(t)|$, $|z_{des}(t)|$, $|\dot{z}_{des}(t)|$ are bounded, one can say that the signals $|\phi(t)|$, $|\theta(t)|$, $|\psi(t)|$, $|z(t)|$ and their time derivatives are bounded by recalling (3.49). Moreover, recalling (3.14)–(3.21) and noting that G is Hurwitz and $|\nu_1(t)|$, $|\nu_2(t)|$, $|\nu_3(t)|$, $|\nu_4(t)|$ are bounded, $|\chi_1(t)|$, $|\chi_2(t)|$, $|\chi_3(t)|$, $|\chi_4(t)|$ are bounded. In view of (2.2) and noting that $\det(W) = \frac{1}{c_\theta} \neq 0$ under Assumption 2 ,$|\omega_1(t)|$, $|\omega_2(t)|$, $|\omega_3(t)|$ become bounded. Therefore, $|\xi_1(t)|$, $|\xi_2(t)|$, $|\xi_3(t)|$, $|\xi_4(t)|$, $|\eta_1(t)|$, $|\eta_2(t)|$, $|\eta_3(t)|$, $|\eta_4(t)|$, $|\eta_{\tau_1}(t)|$, $|\eta_{\tau_2}(t)|$, $|\eta_{\tau_3}(t)|$, $|\eta_{q_1}(t)|$, $|\eta_{q_2}(t)|$, $|\eta_{q_3}(t)|$, $|\eta_{q_4}(t)|$, $|\eta_{r_1}(t)|$, $|\eta_{r_2}(t)|$, $|\eta_{r_3}(t)|$, $|\eta_{r_4}(t)|$ are bounded in consideration of (3.26)–(3.36) and noting that G is Hurwitz. To

show the boundness of $|\eta_{p_1}(t)|$, $|\eta_{p_2}(t)|$, $|\eta_{p_3}(t)|$, $|\eta_{p_4}(t)|$, (3.41)–(3.44) are rewritten as

$$\begin{bmatrix} \eta_{p_1} \\ \eta_{p_2} \\ \eta_{p_3} \\ \eta_{p_4} \end{bmatrix} = T^{-1} \begin{bmatrix} \delta_1 - \chi_1 - \xi_1 - \lambda_1 \eta_{\tau_1} \\ \delta_2 - \chi_2 - \xi_2 - \lambda_2 \eta_{\tau_2} \\ \delta_3 - \chi_3 - \xi_3 - \lambda_3 \eta_{\tau_3} \\ \delta_4 - \chi_4 - \xi_4 + a\eta_a \end{bmatrix} \tag{3.121}$$

where T is given by

$$T = \begin{bmatrix} -p_1 & p_2 & 0 & 0 \\ 0 & 0 & -p_3 & p_4 \\ q_1 & q_2 & -q_3 & -q_4 \\ r_1 & r_2 & r_3 & r_4 \end{bmatrix} \tag{3.122}$$

The determinant of T which is

$$\begin{aligned} det(T) = &- p_1p_3q_2r_4 - p_1p_3q_4r_2 - p_1p_4q_2r_3 - p_1p_4q_3r_2 - p_2p_3q_1r_4 - p_2p_3q_4r_1 \\ &- p_2p_4q_1r_3 - p_2p_4q_3r_1 \end{aligned} \tag{3.123}$$

is not equal to zero since p_1, p_2, p_3, p_4, q_1, q_2, q_3, q_4, r_1, r_2, r_3, r_4 are plant parameters and they are always positive. Therefore, $|\eta_{p_1}(t)|$, $|\eta_{p_2}(t)|$, $|\eta_{p_3}(t)|$, $|\eta_{p_4}(t)|$ are bounded and it is satisfied that $|\Omega_1(t)|$, $|\Omega_2(t)|$, $|\Omega_3(t)|$, $|\Omega_4(t)|$ are bounded in view of (3.50). Moreover, by LaSalle-Yoshizawa theorem, (3.117) ensures that $|e_1(t)|$, $|e_2(t)|$, $|e_3(t)|$, $|e_4(t)|$, $|\delta_1(t)|$, $|\delta_2(t)|$, $|\delta_3(t)|$, $|\delta_4(t)|$ converge to zero as $t \to \infty$. □

3.4. Simulation Results

A simulation is performed on Matlab to test the performance of the controller. The parameters provided in Table 3.1 are used during the simulations. As mentioned in Section 2.3, the wind velocity vector field is selected as

$$V_{wind,x} = -\dot{x} + \frac{y}{\sqrt{x^2+y^2}} \sum_{i=1}^{20} g_{i,x}(z) sin(\omega_{i,x} t + \phi_{i,x}) \tag{3.124}$$

$$V_{wind,y} = -\dot{y} + \frac{x}{\sqrt{x^2+y^2}} \sum_{i=1}^{20} g_{i,y}(z) sin(\omega_{i,y} t + \phi_{i,y}) \tag{3.125}$$

$$V_{wind,z} = -\dot{z} + \sum_{i=1}^{20} g_{i,z}(z) sin(\omega_{i,z} t + \phi_{i,z}). \tag{3.126}$$

where $\dot{x}, \dot{y}, \dot{z}, x, y, z$ are the velocity and the positon of quadrotor with respect to EFF, $g_{i,x}(z), g_{i,y}(z), g_{i,z}(z)$ are the amplitude of corresponding sinusoid which is calculated by Dryden gust model in [11], $\omega_{i,x}, \omega_{i,y}, \omega_{i,z}$ are the frequencies and $\phi_{i,x}, \phi_{i,y}, \phi_{i,z}$ are the phases. Figure 3.1 shows the wind velocity with respect to EFF at a given point.

Table 3.1. Parameter Values Used in Simulations

m=0.52 kg	d_1=6.09 10^{-7} Nms^2/rad^2
J_{11}=7.5x10^{-3} kg/m^2	d_2=6.56 10^{-7} Nms^2/rad^2
J_{22}=7.5x10^{-3} kg/m^2	d_3=7.50 10^{-7} Nms^2/rad^2
J_{33}=1.3x10^{-2} kg/m^2	d_4=7.03 10^{-7} Nms^2/rad^2
b_1=2.54 10^{-5} Ns^2/rad^2	l_1=0.23 m
b_2=2.74 10^{-5} Ns^2/rad^2	l_2=0.23 m
b_3=3.13 10^{-5} Ns^2/rad^2	l_3=0.23 m
b_4=2.93 10^{-5} Ns^2/rad^2	l_4=0.23 m

For the wind observer, it is assumed that the wind has at most three distinct frequencies. Therefore, the controllable pair (G, L) is chosen as $G, L \in \mathbb{R}^7$.

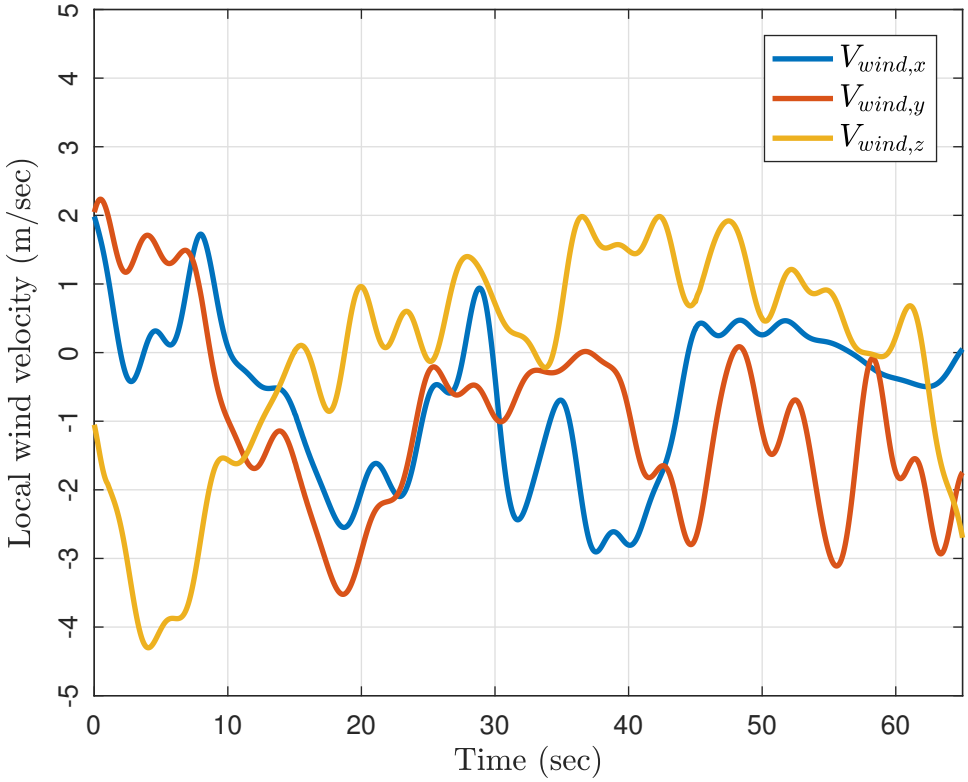

Figure 3.1. Wind velocity vs time at the position (1,1,1) with respect to EFF

Moreover, a trajectory plan is used for any change in each desired state. For example, the $z_{des}(t)$ case is given by;

$$\begin{aligned} z_{des}(t) =& h_0 + h_1(t-t_0)^3 + h_2(t-t_0)^4 + h_3(t-t_0)^5 \\ \dot{z}_{des}(t) =& 3h_1(t-t_0)^2 + 4h_2(t-t_0)^3 + 5h_3(t-t_0)^4 \\ \ddot{z}_{des}(t) =& 6h_1(t-t_0) + 12h_2(t-t_0)^2 + 20h_3(t-t_0)^3. \end{aligned}$$

for $t_0 \leq t \leq t_1$ where t_1 is given, t_0 is the initial time when a state starts going to a desired state, h_0, h_1, h_2, h_3 are the trajectory constants which are calculated by using the given constraints $z_{des}(t_0), z_{des}(t_1), \dot{z}_{des}(t_1), \ddot{z}_{des}(t_1)$. The same task is used for other states.

The simulation results are seen in Figure 3.2. At $t = 15$ sec, one of the propeller rubs somewhere and its drag and thrust force decreases by one third . At $t = 45sec$, an extra mass (0.3kg) is hanged on the quadrotor. Figure 3.3 shows the angular velocities of rotors in time. Since the propellers are chosen as different, the rotors rotates at

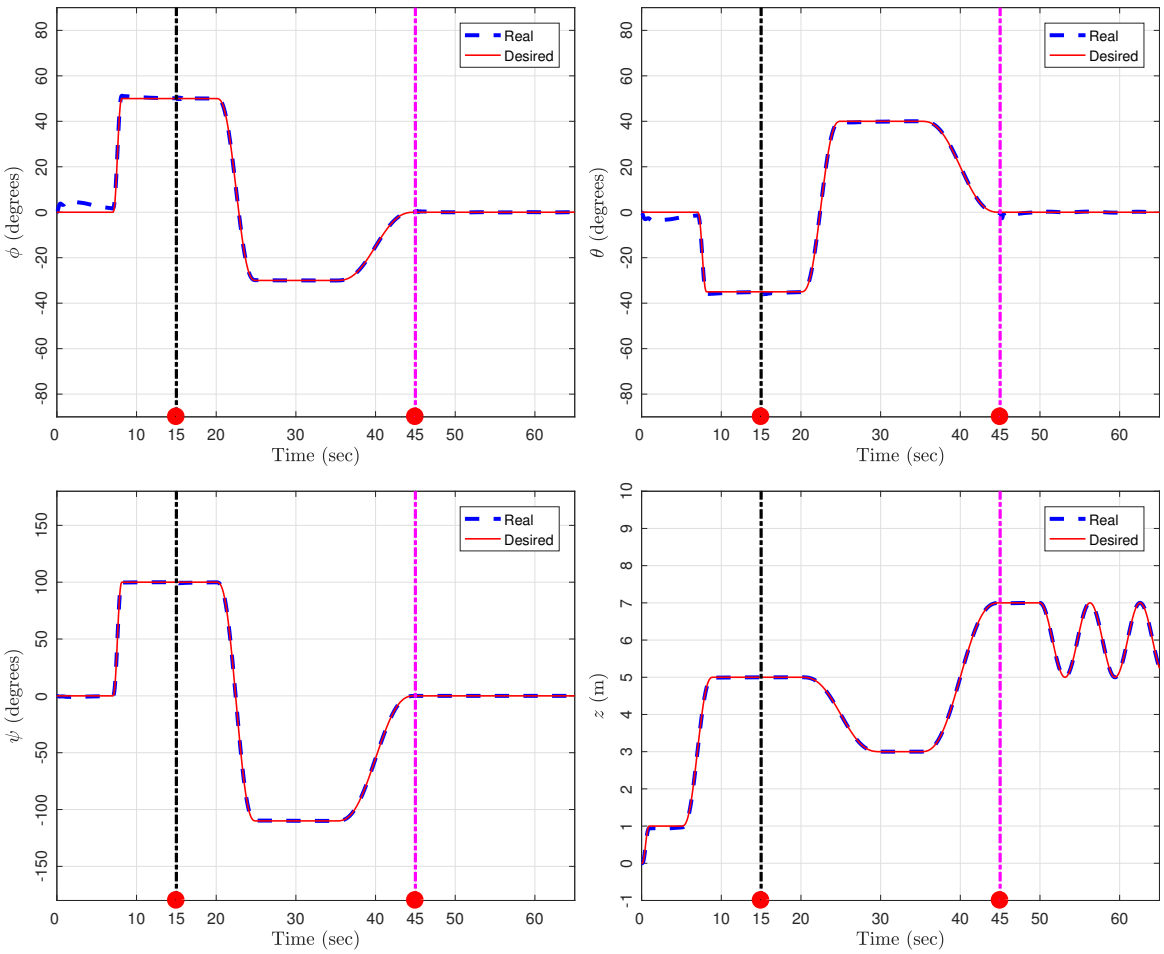

Figure 3.2. MATLAB simulation results. The dashed lines and the solid lines represent the actual states and the desired states, respectively. The vertical dash-dot lines at $t = 15$ sec represent the circumstance when one of the propeller rubs somewhere and its drag and thrust coefficients decrease. The vertical lines at $t = 45$ sec represent the circumstance when extra mass $(0.3kg)$ is hang on the quadrotor.

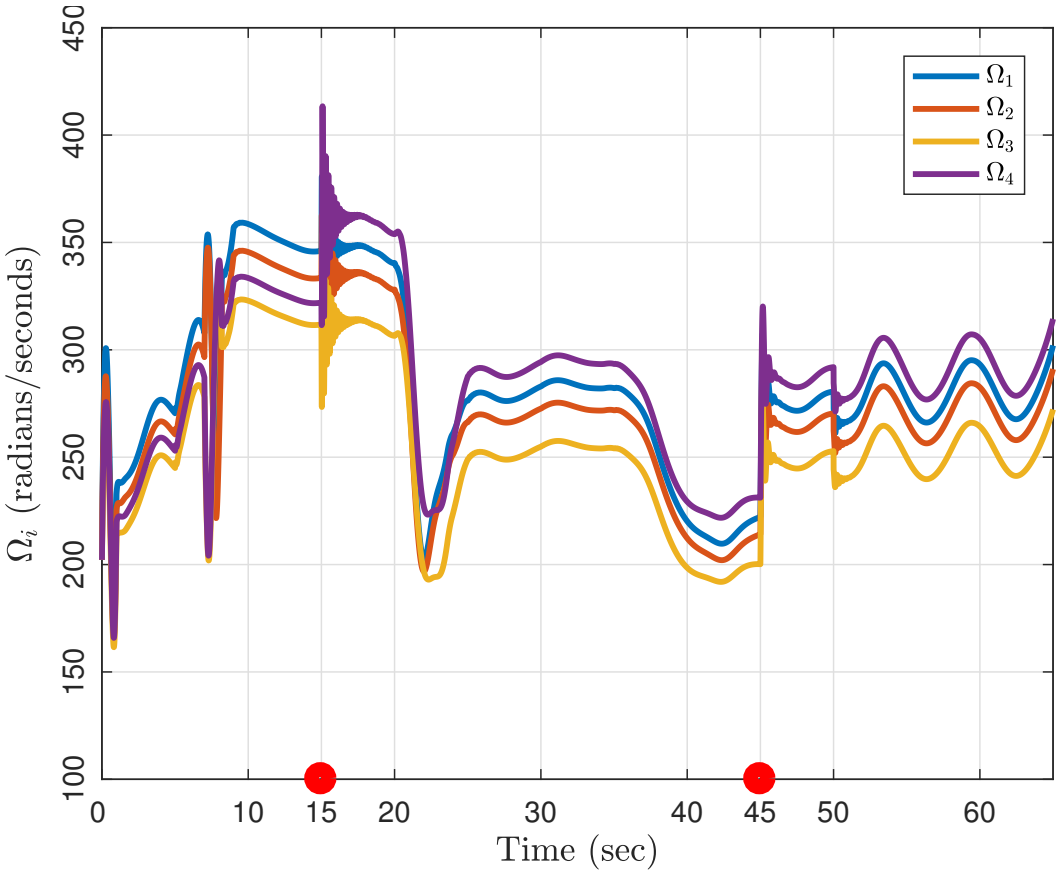

Figure 3.3. Angular velocities of rotors vs Time. Since the propellers are chosen as different, the rotors rotates at different angular velocities in order to satisfy the stability. At $t = 15sec$, the propeller attached to the 4^{th} motor is damaged and its thrust and drag coefficients decrease, thus, its angular velocity increase. At $t = 45sec$, Ω_i increase due to the fact an extra mass is hanged on the center of the quadrotor.

different angular velocities in order to satisfy the stability. At $t = 15$ sec, the propeller attached to the 4^{th} motor is damaged and its thrust and drag coefficients decrease, thus, its angular velocity increase.At $t = 45$ sec, Ω_i increase due to the fact an extra mass is hanged on the center of the quadrotor.

As it is seen from Fig 3.2, the Euler angles and the altitude of quadrotor converge to desired values despite wind disturbances. Moreover, since the small angle approximation is not used, the pitch and the roll angles can reach more than 20 degrees where the linear relationship between an angle and its sine disappears. With these results, it is shown that the boundness and convergence of the signals are achieved as Theorem 3.2 states.

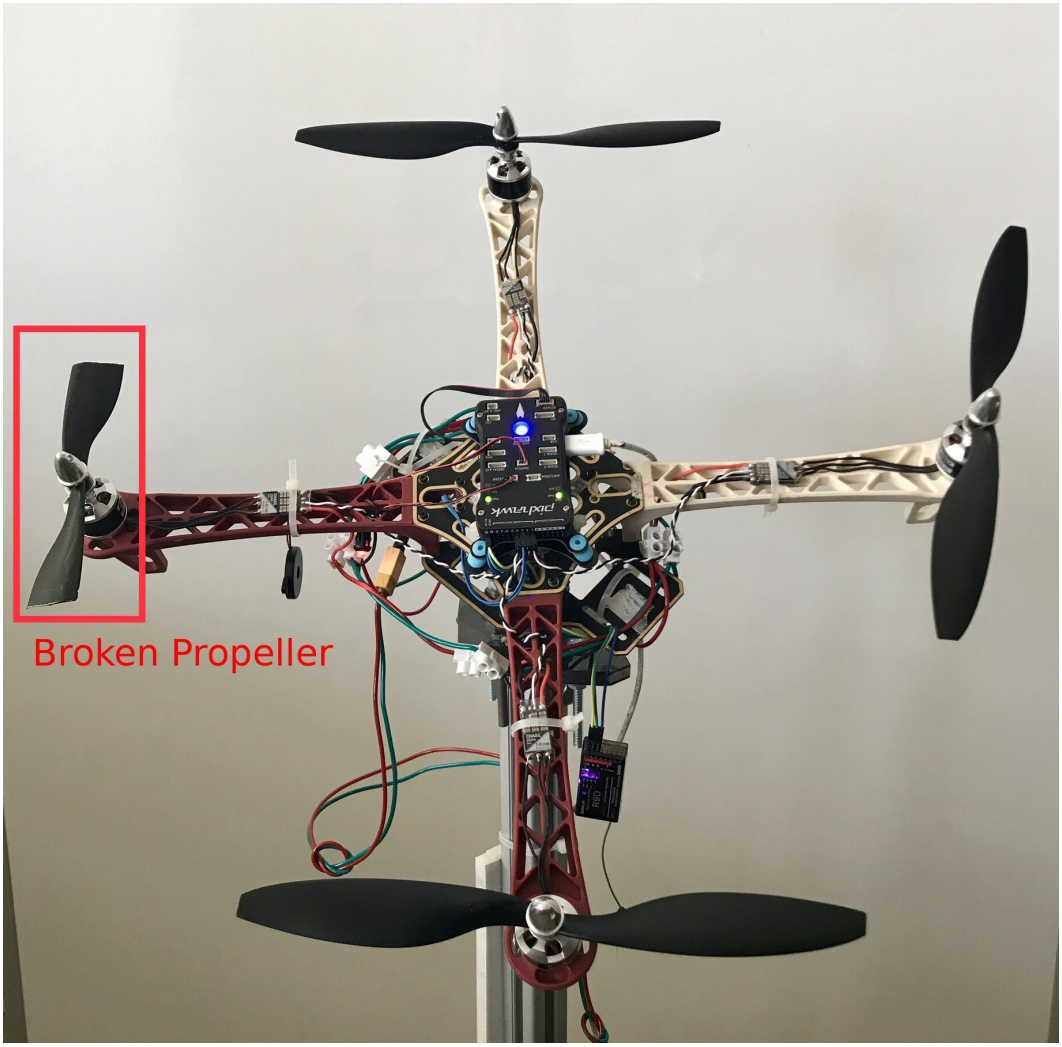

Figure 3.4. Experimental setup for the comparison between the performances of PID and the designed adaptive controller. As seen, the propeller on the left is broken.

3.5. Experimental Results

In the experiment, the setup in Figure 3.4 is used. As seen in Figure 3.4, one of the propellers is broken so that the performance of conventional PID controller and the designed adaptive controller despite system uncertainty is compared.

In the setup, Pixhawk microcontroller is used. Pixhawk is an independent project aiming at providing high-end industry standard autopilot hardware to the academic, hobby and industrial communities at low costs and high availability. There are two open-source code stacks for Pixhawk which are ArduPilot and PX4. Both are written in C++. In this experiment, ArduPilot flight code stack is used as it is easier to be

modified compared to PX4.

ArduPilot consists more than 20 flight modes for quadrotors. A flight mode determines how quadrotor is controlled. For example, when stabilize flight mode is active, quadrotor receives reference roll, pitch angles, yaw angle rate and total thrust signals or when PosHold mode is active, quadrotor automatically attempts to maintain its current location, heading and altitude. In the experiment, stabilize flight mode is used. Both controllers (PID and adaptive controller) attempt to keep the attitude of the quadrotor regarding to the reference signals.

In the experiment, only the thrust signal is changed. Therefore, the attiude of quadrotor should be kept same despite the broken propeller seen in Figure 3.4. In other words, the quadrotor should be always parallel to horizontal plane when the total thrust changes. The result is as seen Figure 3.5. Until 17 seconds, the conventional PID controller is active, after that, the adaptive controller steps in. Figure 3.5 shows the difference on their performances. The PID controller can not adapt itself to the change in the parameters (in this case, it is a broken propeller), hence, it misses reference signals every time the total thrust signal changes. However, the adaptive control adapts itself to the change (in other words, it identifies the uncertainty and acts to handle that problem) and tracks the reference signals better. The root mean square errors of both controllers can be seen in Table 3.2.

The video of this experiment can be seen in [49].

Table 3.2. Root Mean Square Error Comparison

	PID	Adaptive
ϕ	9.3217	0.7118
θ	0.7290	0.7227
ψ	4.2474	2.3919

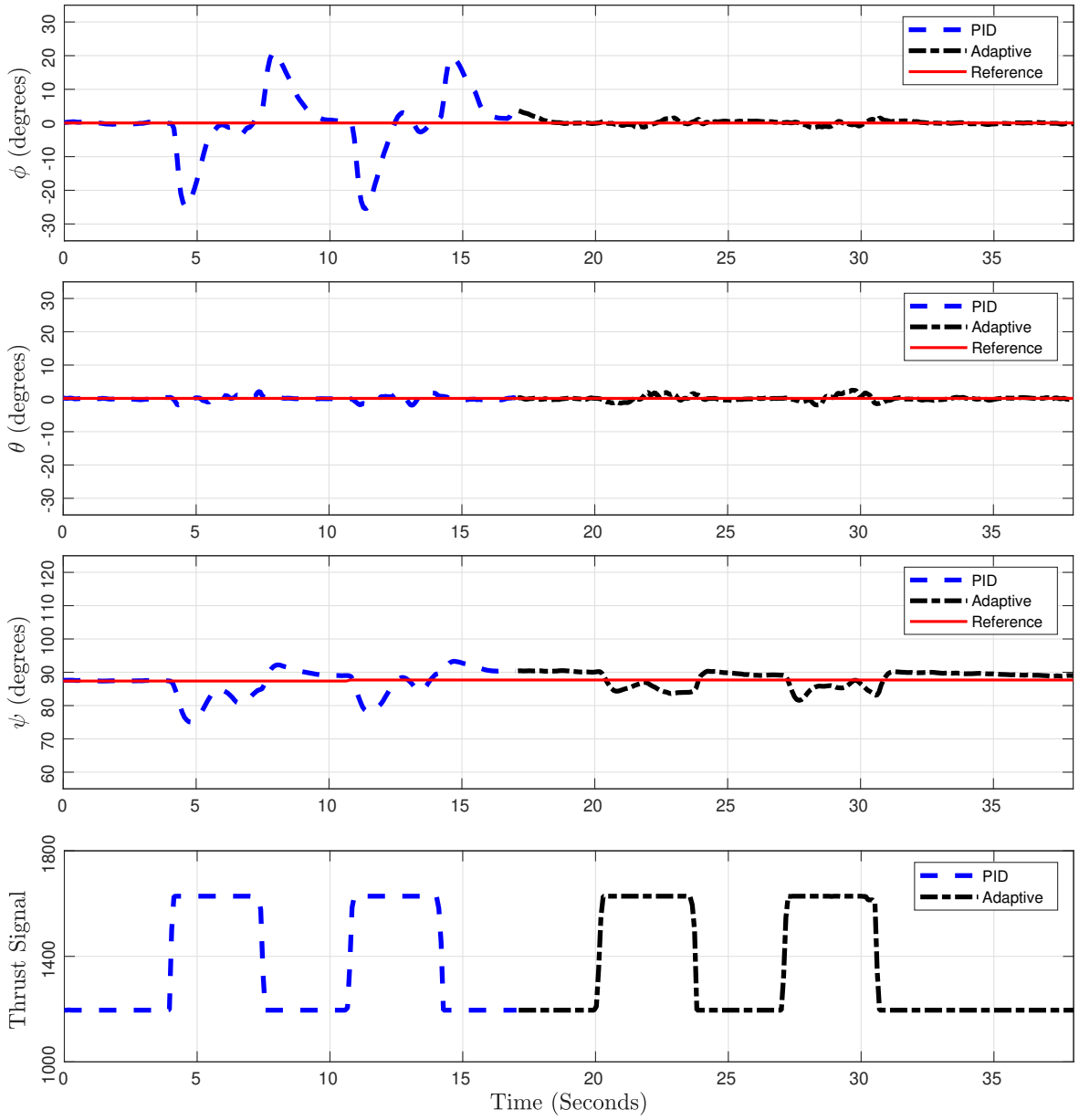

Figure 3.5. Results of the experiment. Until 17 seconds, PID controller is active. During the rest, the adaptive controller is active. As it is seen in the first graph, PID controller can not adapt itself despite the uncertainty in system parameters which is the broken propeller in this case. However, the adaptive controller performs better than PID and keeps the stability of the system.

4. EXTREMUM SEEKING CONTROLLER DESIGN

Extremum seeking control is a non-model-based real time optimization tool to find maximum or minimum points, whether absolute or local, of a function without the knowledge of its shape by perturbing the input of the function. While designing the controller algorithm, extremum seeking for a static map in [31] is utilized and its stability is proven by using averaging method in [50].

In the experiment, it is assumed that a light source, the yellow circle in Figure 4.1, creates a signal map and the luminosity value, illustrated as red background in the figure, decreases gruadually as it is moved away from the light source. The signal map $S = f(\psi_s)$ on the circle line whose radius L is the distance between the quadrotor's center and the sensor is a function of the position of the light sensor ψ_s. The maximum value of $S^* = f(\psi_s^*)$ is at ψ_s^* which is the closest point of the light sensor to the light bulb where the luminosity value is maximum as seen Figure 4.1. The aim of the designed extremum seeking controller is to drive the quadrotor's yaw angle ψ to ψ_s^* without the knowledge of the signal map S by perturbing the angular position of the light sensor ψ_s on top of the quadrotor and measuring the luminosity value $S = f(\psi_s)$.

4.1. Controller Algorithm

The entire control loop can be examined by dividing it into three main sections as it is shown in Figure 4.2. In the first section numbered as 1 encircled with red dashed line, a basic extremum seeking loop which is identical to the one in the reference [31] can be seen. In this experiment, the nonlinear signal map refers to the distribution of the luminosity which decays away from the source. With respect to the experimental setup, the maximum point of the luminosity, S^*, is found in front of the light bulb ψ^* as seen in Figure 4.1. The luminosity sensor ,which is translocated in the inertial frame by the quadrotor's angular movement and the servo motor's rotation, measures the local luminosity value $S(\psi_s)$ in the signal map. The position of the sensor with respect to the ground can be seen as ψ_s in Figure 4.2. The nonlinear signal map gives

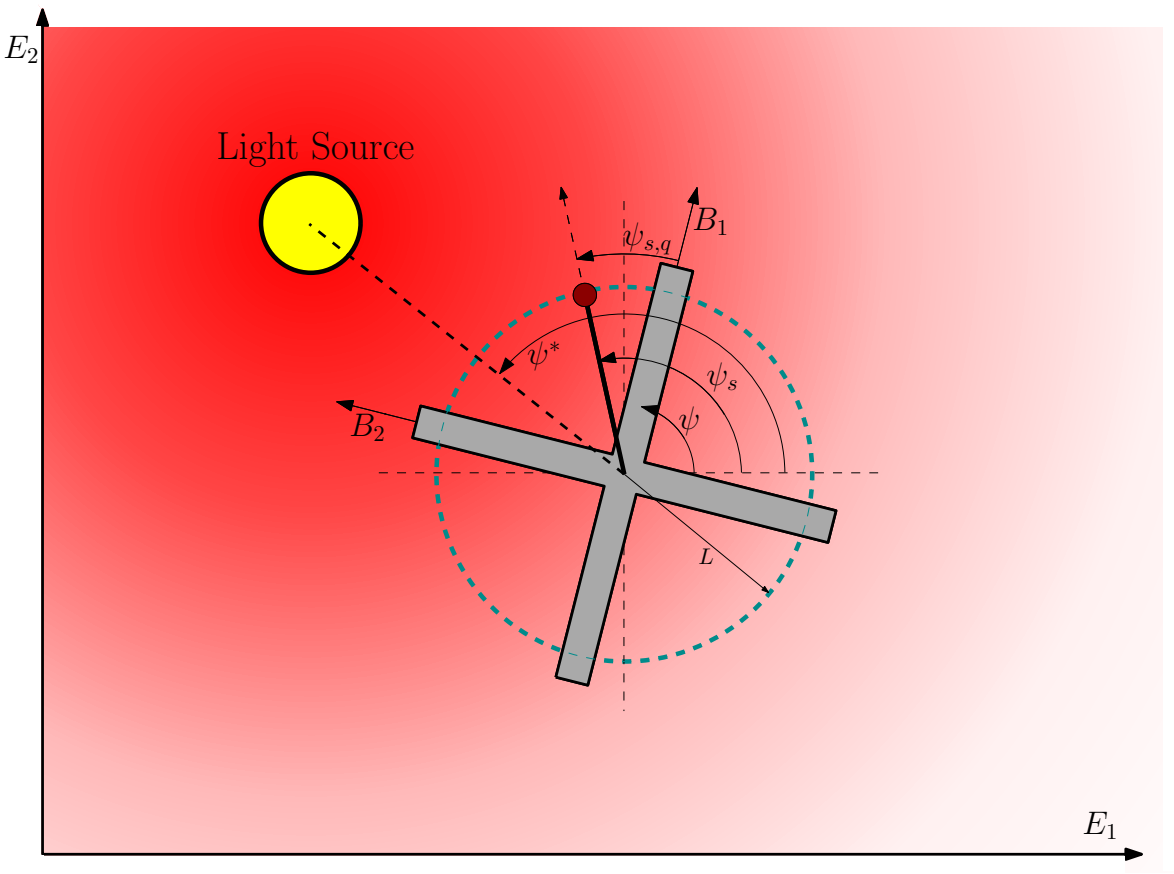

Figure 4.1. Scheme of the quadrotor. In this scheme, the quadrotor and the arm of the servo motor are illustrated in a nonlinear signal map formed by a light source. The quadrotor's forepart looks towards the positive B_1 axis. The red sphere symbolizes the luminosity sensor at the tip of the servo motor's arm.

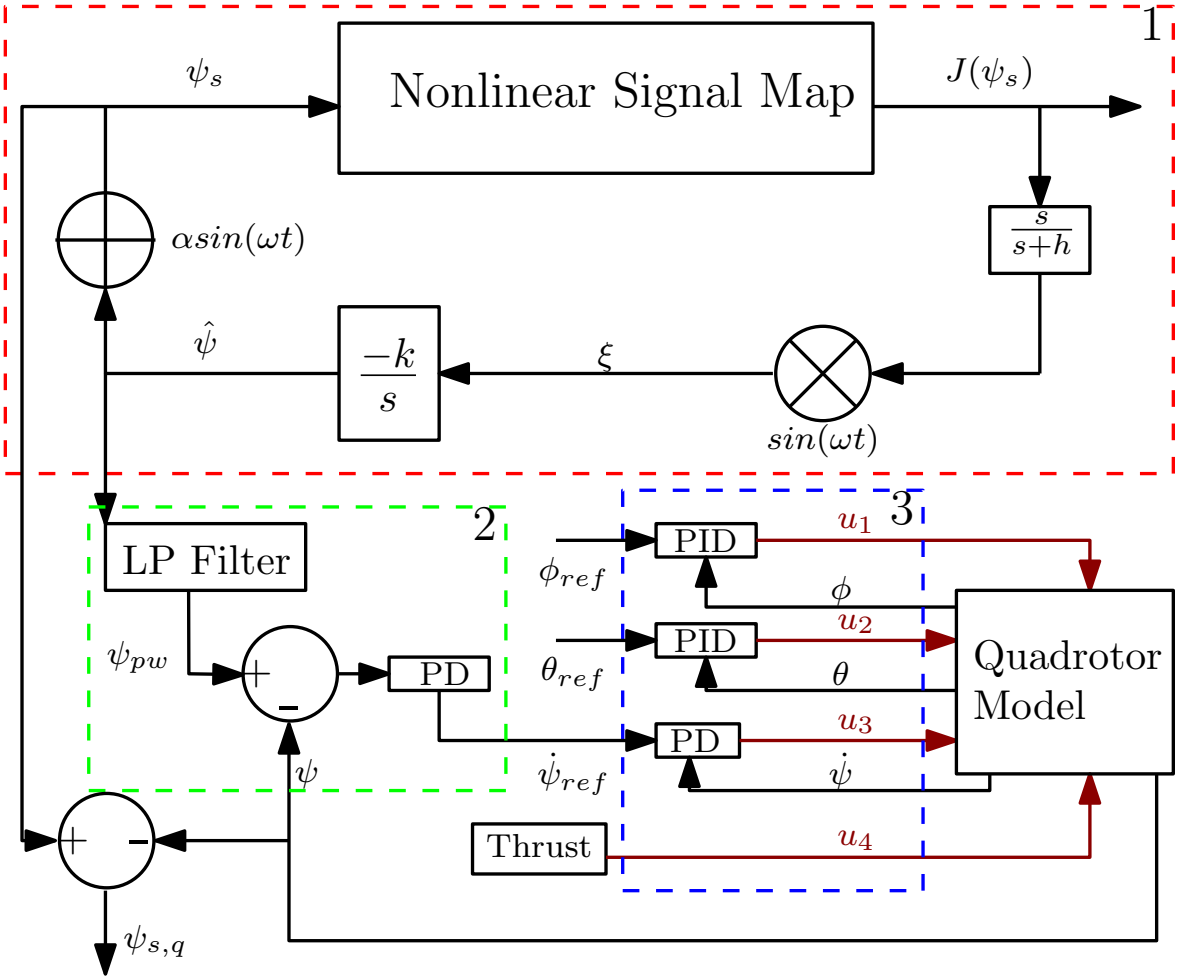

Figure 4.2. Extremum seeking control loop. The entire loop is divided into three sections. Section 1 is Extremum Seeking Loop for Static Map, Section 2 is Reference Yaw Rate Control Loop for Quadrotors and Section 3 is Ardupilot Control Loop in Pixhawk.

a luminosity value $S(\psi_s)$ corresponding to the position of the sensor whose function can be written as,

$$S(\psi_s) = S^* + \frac{S''}{2}(\psi_s - \psi^*)^2, \tag{4.1}$$

where S'' is the second derivative of the signal map. By using the equalities $\tilde{\psi} = \psi^* - \hat{\psi}$ and $\psi_s - \psi^* = \alpha \sin(\omega t) - \tilde{\psi}$ where $\alpha \sin \omega t$ is the perturbation signal, $\hat{\psi}$ is the estimate of the unknown optimal input, $\tilde{\psi}$ is the estimation error, (4.1) is rewritten as,

$$S(\psi_s) = S^* + \frac{S''}{2}(\tilde{\psi}_s - \alpha \sin \omega t)^2. \tag{4.2}$$

By applying a basic trigonometric identity which is $2\sin^2(\omega t) = 1 - \cos(2\omega t)$, the equation (4.2) is transformed to,

$$S(\psi_s) = S^* + \frac{\alpha^2 S''}{4} + \frac{S''}{2}\tilde{\psi}^2 - \alpha S''\tilde{\psi}\sin(\omega t) + \frac{\alpha^2 S''}{4}\cos(2\omega t). \tag{4.3}$$

This measurement is transfered to the Arduino and introduced to the extremum seeking loop.

At first, the measured value is crossed through a washout filter, which is a high-pass filter, to clean the DC component of the measurement [31]. Then the filtered data is demodulated by a perturbation signal, $\sin(\omega t)$, to form an estimation of the derivative, ξ which is given by

$$\begin{aligned}\xi =& \frac{s[S]}{s+h}\sin \omega t \approx -\frac{\alpha S''}{2}\tilde{\psi} + \frac{\alpha S''}{2}\tilde{\psi}\cos 2\omega t + \frac{\alpha^2 S''}{8}(\sin \omega t - \sin 3\omega t) \\ &+ \frac{S''}{2}\tilde{\psi}^2 \sin \omega t\end{aligned} \tag{4.4}$$

with a identity which is $2\cos 2\omega t \sin \omega t = \sin 3\omega t - \sin \omega t$. Noting that ψ^* is constant and $\dot{\tilde{\psi}} = -\dot{\hat{\psi}}$, the equation for $\dot{\tilde{\psi}}$ can be obtained as follows,

$$\dot{\tilde{\psi}} = k\xi \approx -\frac{k\alpha S''}{2}\tilde{\psi} + \frac{k\alpha^2 S''}{8}(\sin(\omega t) - k\sin(3\omega t)) + \frac{k\alpha S''}{2}\tilde{\psi}\cos(2\omega t) + \frac{kS''}{2}\tilde{\psi}^2\sin(\omega t) \tag{4.5}$$

By averaging the equation (4.5) as stated in [50], it is obtained a much simpler equation as,

$$\dot{\tilde{\psi}}_{av} \approx -\frac{k\alpha S''}{2}\tilde{\psi}_{av}. \tag{4.6}$$

By integrating ξ with $\frac{-k}{s}$, $\hat{\psi}$ is obtained as,

$$\hat{\psi} \approx -\frac{k}{s}\left[-\frac{\alpha S''}{2}\tilde{\psi}\right] \tag{4.7}$$

The sign of the k defines the direction of the estimate, $\hat{\psi}$. In the experiment, the k is taken as positive with the aim of converging to the maximum point of the nonlinear signal map which is the light source. In an opposite case, it must be taken as negative. As a result, the system is stable and $\tilde{\psi} \to 0$ as $kS'' > 0$.

The magnitude of the k also plays an important role in the convergence rate. As the gain parameter k increases, the speed of convergence to the light source is rising [31]. Nevertheless, there is an upper limit for the gain parameter to restrict the sensitivity of the system to the small variations in Non-Linear Signal Map. Actually, the more sensitivity is desired when the system is far away from the maximum point

of signal map. However, this sensitivity brings a drawback when the system is near by the maximum point, such as a deviation, from the extremum, which stems from small changes in the signal map measurements.

After the integrator, another perturbation, $\alpha sin(\omega t)$ is added to $\hat{\psi}$. The contribution of this perturbation is to expand the region of scanning in the signal map [31]. As the parameter α increases, the scanned region also increases and the sensor measurements between the two edges of the region depart from each other. This difference between the two edges also makes a contribution to the speed of convergence. However, the gain in the speed of convergence is limited by the mechanical boundaries of the servo motor. The restricted rotation capability between zero to three hundreds degrees of the servo motor defines the natural boundaries of the instantaneous region of scanning. Therefore, increasing the parameter α after an upper limit is inconclusive. The last parameter is the perturbation frequency, ω. In the experiment, it is taken as $\frac{\pi}{\Delta t}$, where Δt is the elapsed time during the processing of one loop in Arduino. Eventually, the value of $\sin(\omega t)$ varies between 1 and -1 in every successive loop and the servo motor can achieve the oscillatory motion. Since the servo motor is fixed on the quadrotor as it can be seen in Figure 4.1, the given input which is sent to the motor should be the position of the servo motor with respect the quadrotor, $\psi_{s,q}$. To acquire this input, quadrotor's angular position with respect to the inertial frame, ψ, is subtracted from evaluated ψ_s. The signal, ψ is measured by Pixhawk's own gyro. Finally the servo motor is steered by Arduino to the obtained $\psi_{s,q}$ angle.

In the second section of the entire control loop, encircled with the green dashed line and numbered 2, a reference yaw rate $\dot{\psi}_{ref}$ for Pixhawk micro-controller is evaluated for the rotation of the quadrotor in order that the forepart of the quadrotor tracks the light source. As it is wanted to track a consistent reference, instead of the fluctuating motion of the servo motor ψ_s , the estimate, $\hat{\psi}$, with shorter fluctuations is chosen as the reference and it is also passed through a low pass filter to obtain a smoother one. The acquired value ψ_{pw} shows the reference yaw with respect to the inertial frame. To evaluate the reference yaw rate of the quadrotor $\dot{\psi}_{ref}$ to track the reference pathway in a smooth beahvior, it is used a PD controller which expects an error value. The error

is defined as the difference between the reference yaw ψ_{pw} and the quadrotor's yaw ψ both with respect to the inertial frame.

Lastly, in the third section which is encircled with the blue dashed line and numbered 3 in Figure 4.2, the conventional control algorithm in Pixhawk flight controller is basically represented. The "stabilize" flight mode of Pixhawk is utilized which means that the inputs are sent as reference roll angle ϕ_{ref}, reference pitch angle θ_{ref}, reference yaw angle rate $\dot{\psi}_{ref}$ and thrust u_4. In the system, the reference roll angle $\phi_{ref} = 0$, the reference pitch angle $\theta_{ref} = 0$ to hold the quadrotor parallel to the horizontal plane, the thrust u_4 is given by the pilot manually and the reference yaw angle rate $\dot{\psi}_{ref}$ is evaluated in the extremum seeking loop in Arduino as mentioned before. The control inputs u_1, u_2, u_3 are calculated with the help of PID control algorithms regarding to the errors between the Euler angles of the quadrotor and their references. Since the last control input u_4 is given by the pilot manually, the angular speed of rotors Ω_i^2 can be calculated. Although the values of p and q are unknown, they are estimated to some value in Pixhawk flight controller as their value can be compensated by PID gains used in the calculations of u_i.

To sum up, it is obtained a reference pathway by performing extremum seeking with the help of luminosity sensor and the servo motor. Then yaw motion of the quadrotor is controlled in the manner that the forepart tracks this reference. As the servo motor is directed towards the light source by the extremum seeking, the reference also leads the quadrotor to the light bulb's face.

4.2. Experimental Setup

As it can be seen in Figure 4.3, the quadrotor is anchored from the bottom of its main body and is allowed solely to revolve around itself by the ball joint connection. Therefore, the quadrotor cannot move horizontally and vertically. The motion of the quadrotor is controlled by Pixhawk flight controller, which can be seen in Figure 4.4, according to the reference pitch and roll angles, the reference yaw rate and thrust input. The two reference angles, the pitch and the roll, and the thrust input are sent

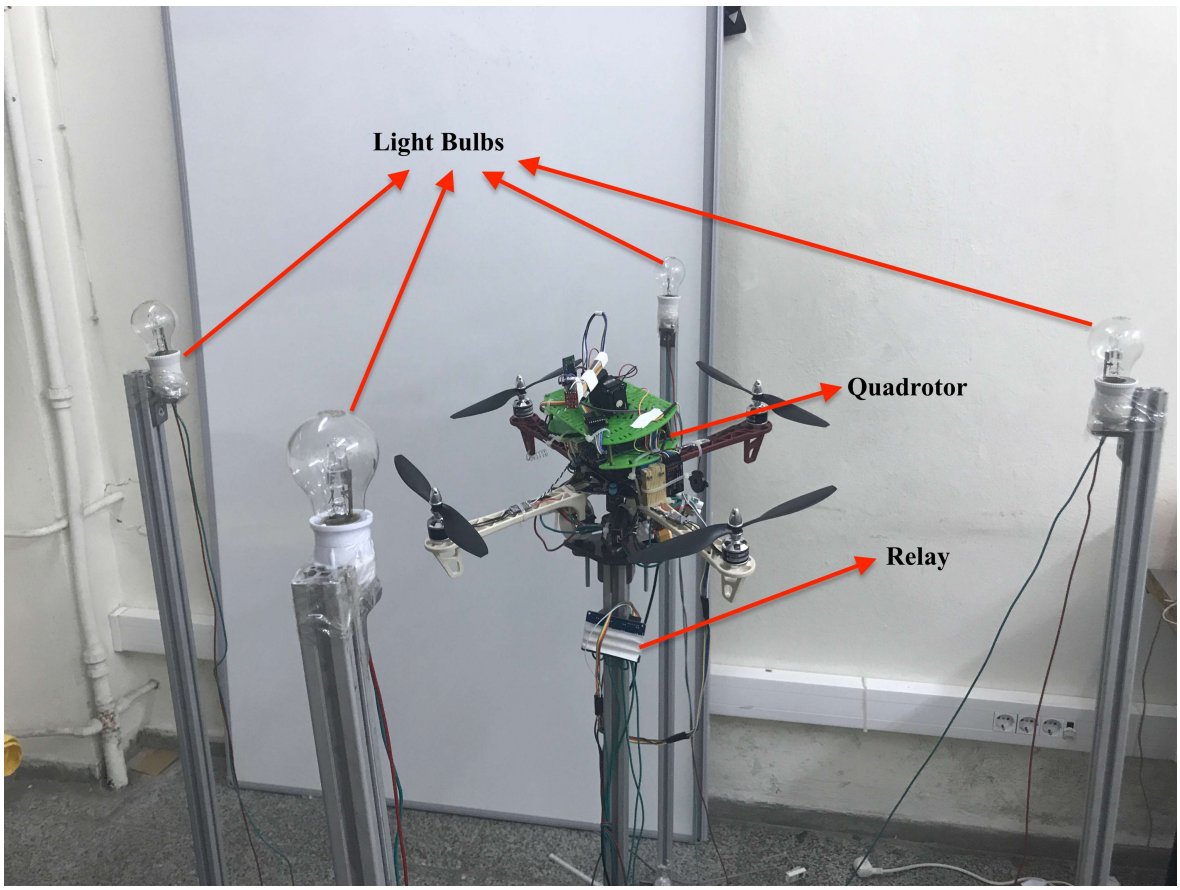

Figure 4.3. Setup of the Experiment. In this figure the entire experimental setup can be seen. Around the fixed quadrotor four light bulbs are placed at equal distances with ninety degrees differences. They are lighted on and off respectively by a relay and it is expected that the quadrotor's forepart will track the active light source by the extremum seeking.

from the RC receiver. The reference yaw rate is evaluated in Arduino with respect to the extremum seeking and forwarded to Pixhawk.

The extremum seeking in Arduino is performed through the instrument of the information obtained by SparkFun TSL2561 luminosity sensor which is mounted on the tip of an arm governed by a Dynamixel AX-12A servo motor as it can be seen in Figure 4.4. The servo motor is fixed on the quadrotor as in Figure 4.4 and driven by Arduino according to the extremum seeking. In addition to the luminosity sensor which is used for the extremum seeking, another one is fixed at the quadrotor's forepart in order to confirm whether the quadrotor is converging to the maximum point of the signal map

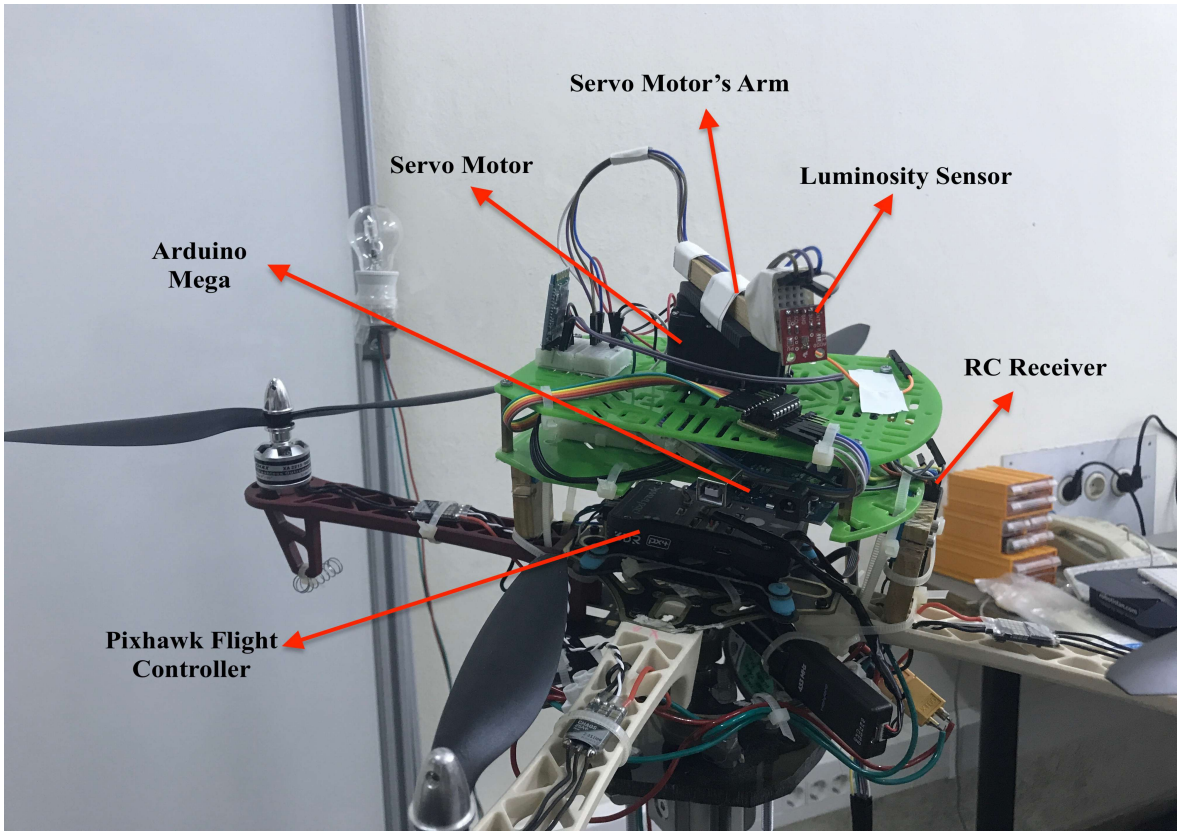

Figure 4.4. Equipments used for the Extremum Seeking

or not.

In the experiment, as the reference yaw rate is evaluated in Arduino instead of being sent from the RC, it is transmitted through an independent channel from Arduino as a PWM (Pulse Width Modulation) signal. Moreover, the reference roll angle, the reference pitch angle and the thrust information are transmitted as PWM signals through three different channels from the RC receiver. Since Pixhawk flight controller uses the SBUS as the serial communication way, all the channels which deliver different informations via PWM signals are collected and transformed to SBus communication protocol in a PWM to SBUS converter.

As it can be seen in Figure 4.3 the lighting arrangement around the fixed quadrotor consists of four lighting bulbs placed on the same circular trajectory with a specific distance R from the quadrotor and spaced by ninety degrees from each other. By lighting on and off the bulbs in different patterns which is unknown for the extremum

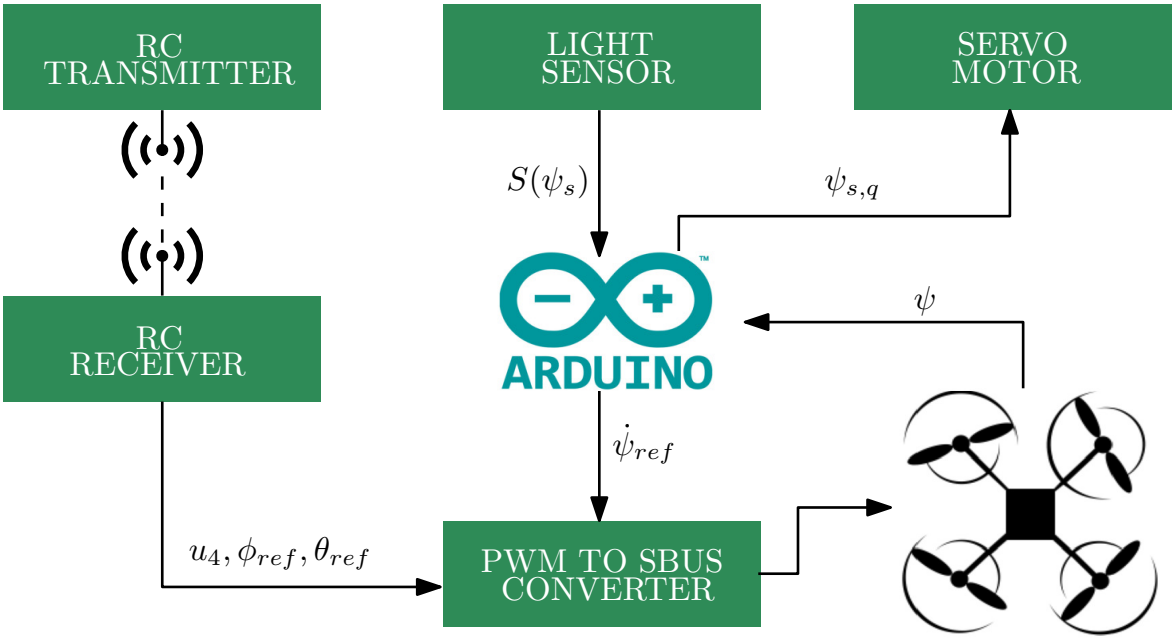

Figure 4.5. System configuration diagram. Arduino takes data from the light sensor, processes the extremum seeking loop and finds the following angular position of the servo motor's arm. This value and the other values (the reference pitch angle, roll angle and the thrust value) from the RC are unified sent to the Pixhawk.

seeking algorithm, the quadrotor's tracking behaviour to the changes in the signal map is observed.

4.3. Result

In the following experiments, the parameters of the extremum seeking are set as $k = 15$, $\alpha = 60$ and ω is defined by the processing time consumed for one loop in the Arduino, in the form of $\omega = \frac{\pi}{\Delta t}$. The elapsed time is measured in Arduino.

The starting angular position of the quadrotor's forepart and the maximum point of the nonlinear signal map are $\psi_0 = \psi_0^* = 0$. Firstly in the experiment, the light bulbs with ninety degrees seperation are lighted on and off respectively in the counterclockwise direction. After a full rotation, they are lighted in the opposite direction. Active light bulb is changed approximately in every twenty-two seconds. As shown in Figure 4.6(a), the quadrotor can react quickly to the change in the position of the light source

and can successfully track the active light source. In Figure 4.6(b) the lux value corresponding to the angular position of the quadrotor's forepart is shown. The system converges successfully to the maximum point of the signal map in every light changing.

The red line in Figure 4.6(a) represents the angular position of the maximum luminosity point with respect to the inertial frame, the blue dashed line exhibits the angular position of the quadrotor's forepart with respect to the inertial frame. In this experiment the angular position of the light source is shifted by ninety degrees in every step and the tracking motion of the quadrotor to catch the light source is observed. In Figure 4.6(a), the quick reaction of the quadrotor as a response to the change in the position of the light source and the smooth converge of ψ to the new position, ψ^*, can be seen. In Figure 4.6(b), this plot shows the lux value measured by the luminosity sensor placed at the forepart of the quadrotor. As it can be seen, in every light changing the measured lux value drops down and then climbs up to the maximum by the quadrotor tracking. The differences between the maximums stems from the differences between the light sources.

A video which is recorded simultaneously with the data shown in the results can be seen in [51].

Also, the video of the other experiment where the quadrotor which is not anchored so that it can freely move in space can be seen in [52]. In the experiment, it is desired that the quadrotor gets closer to the source by giving a constant forward motion signal to the vehicle. Its yaw angle is determined by extremum seeking algorithm so that the quadrotor can be in a small circle area whose center is the source with a constant forward motion. However, it is not explained in detail in this thesis due to the lack of the data and it is not an aim of this thesis. The screenshot of the video can be seen in Figure 4.7.

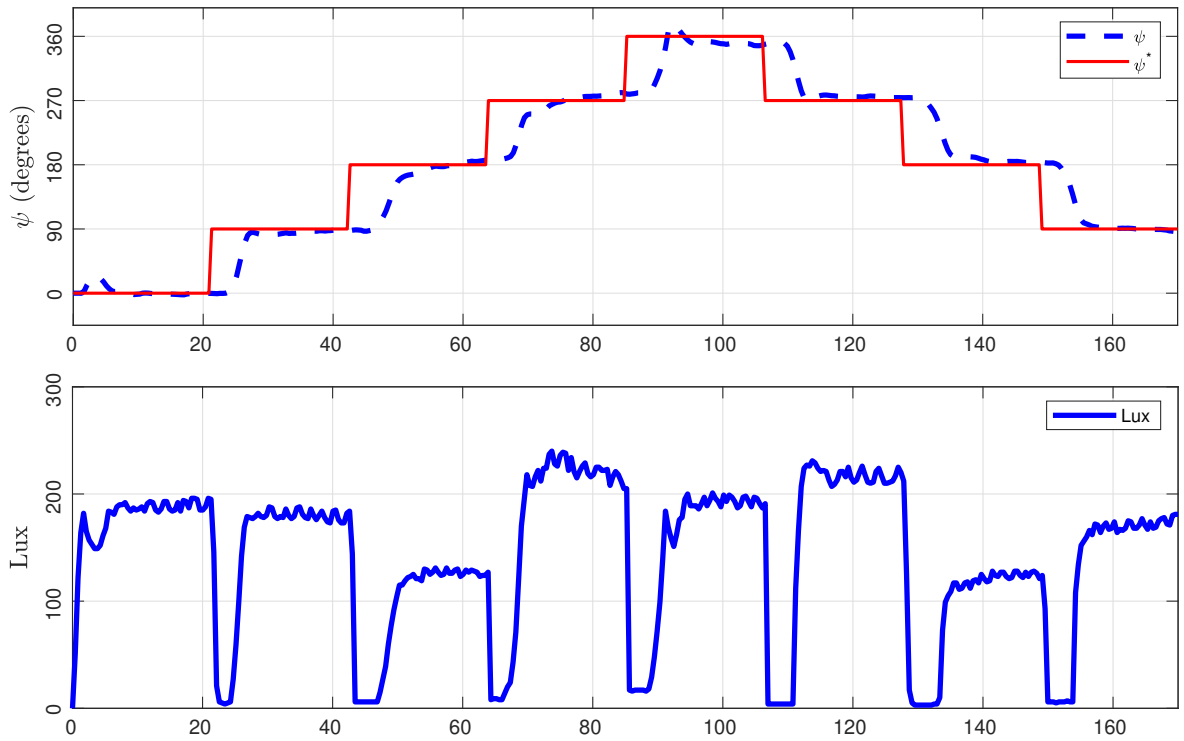

Figure 4.6. Experimental results for the light source tracking of the quadrotor. The red line in the upper figure represents the angular position of the maximum luminosity, the blue dashed line exhibits the angular position of the quadrotor. The second figure shows the lux measured by the sensor at the forepart of the quadrotor.

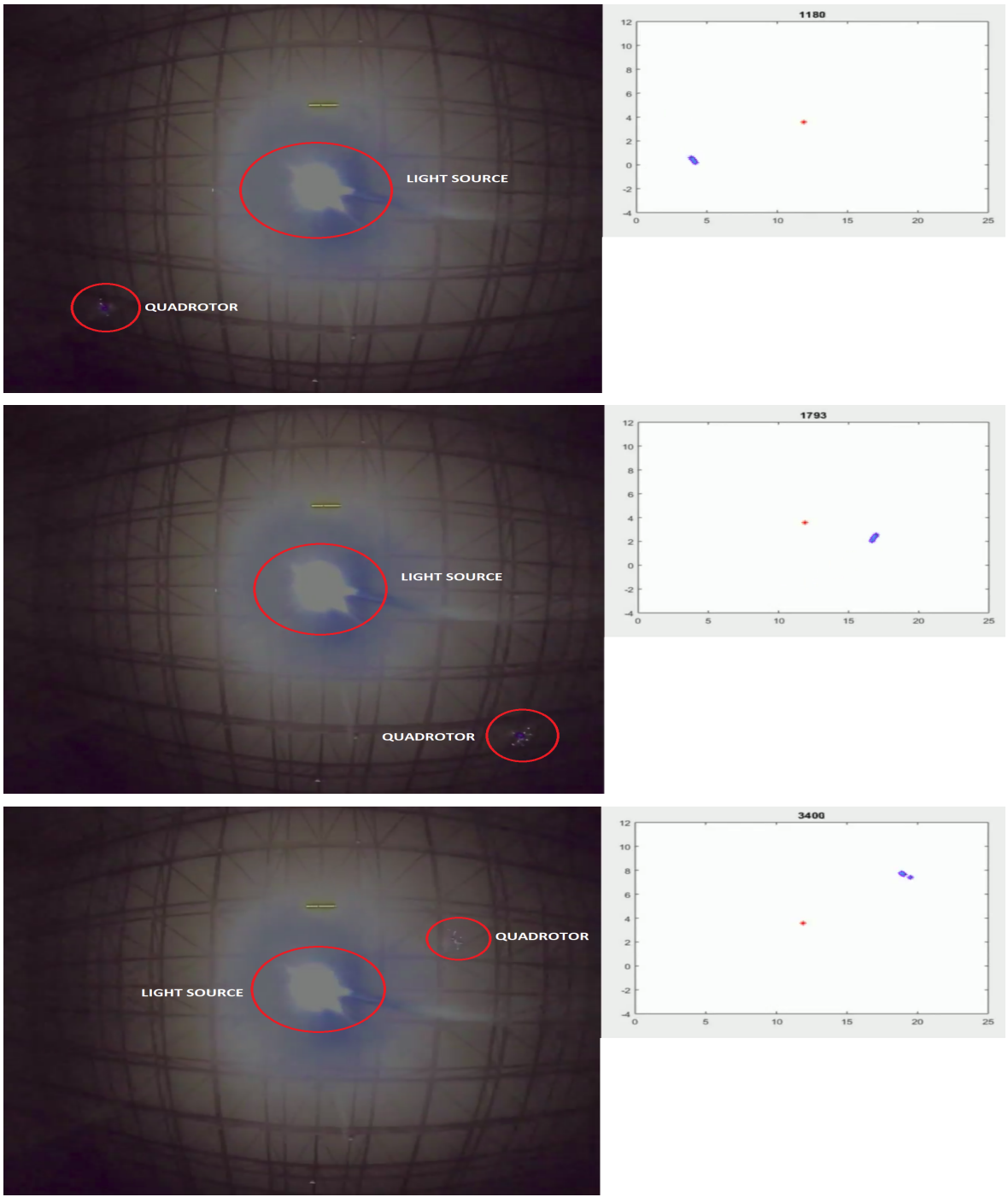

Figure 4.7. Extremum seeking experiment in a basketball field. The quadrotor with the extremum seeking algorithm and equipment moves in a circular area whose center is the light source.

5. CONCLUSION

In this study, two designs for quadrotors have completed. The first is an adaptive controller design and the second is extremum seeking algorithm design.

For the first design, the mathematical model is created in a more realistic way by taking the wind disturbance as a sum of sinusoidal function. Besides, all the system parameters are assumed as unknown. First, observers for wind disturbance are formed. Then, the controller with the observers are designed and the stability of the closed loop system is proved. To show the feasiblity of the controller, a simulation is performed. In that simulation, the wind velocity is taken as sinusoidal changing function, therefore, the wind effect on quadrotor can be considered more realistic. Moreover, different cases are simulated to see that the controller can adapt itself to changes in structural parameters. As seen in Figure 3.2, the attitude and altitude of quadrotor can be controlled with the new adaptive design. To figure out the advantages of the adaptive controller, an experiment is conducted. In the experiment, PID which is the most conventional controller for quadrotors and the designed adaptive controller are compared for the situations of uncertainty in system parameters. By looking at the Figure 3.5, it can be concluded that the designed adaptive controller performs better than the conventional PID contoller and promises a better flight experience.

For the second design, the extremum seeking algorithm is used to drive quadrotor's front to the light source. It is assumed that a light source creates a nonlineaer signal map around itself and the intensity of the light decreases as the distance from the source increases. With this assumption, quadrotor is equipped with extremum seeking hardware seen in Figure 4.4 and algorithm in Figure 4.2 to find the maximum light intensity in this lighted up environment. The experimetal setup in Figure 4.3 is used to show the performance of the algorithm. As seen in Figure 4.3 and Video [51], the quadrotor turns its front to the light source by extremum seeking algorithm.

REFERENCES

1. Taylor, J. and K. Munson, *Jane's pocket book of remotely piloted vehicles: robot aircraft today*, Collier Books, 1977, `https://books.google.com.tr/books?id=8o9TAAAAMAAJ`, accessed at May 2018.

2. Keane, J. F. and S. S. Carr, "A Brief History of Early Unmanned Aircraft", *Johns Hopkins APL Technical Digest*, pp. 559–570, 2013.

3. Chao, H., Y. Cao and Y. Chen, "Autopilots for small unmanned aerial vehicles: A survey", *International Journal of Control, Automation and Systems*, Vol. 8, No. 1, pp. 36–44, February 2010, `https://doi.org/10.1007/s12555-010-0105-z`.

4. Gupte, S., P. I. T. Mohandas and J. M. Conrad, "A survey of quadrotor Unmanned Aerial Vehicles", *2012 Proceedings of IEEE Southeastcon*, pp. 1–6, March 2012.

5. Sarris, Z. and S. Atlas, "Survey of UAV applications in civil markets", *Proceedings of the 9th Mediterranean Conference on Control and Automation*, pp. 1–11, 2001.

6. Lim, H., J. Park, D. Lee and H. J. Kim, "Build your own quadrotor: Open-source projects on unmanned aerial vehicles", *IEEE Robotics & Automation Magazine*, Vol. 19, No. 3, pp. 33–45, 2012.

7. Bouabdallah, S., "Design and control of quadrotors with application to autonomous flying", p. 155, 2007.

8. Bouabdallah, S., A. Noth and R. Siegwart, "PID vs LQ control techniques applied to an indoor micro quadrotor", *2004 IEEE/RSJ International Conference on Intelligent Robots and Systems (IROS) (IEEE Cat. No.04CH37566)*, Vol. 3, pp. 2451–2456 vol.3, September 2004.

9. Jeyaraman, S., A. Tsourdos, R. Zbikowski and B. White, "Formal techniques for

the modelling and validation of a co-operating UAV team that uses Dubins set for path planning", *American Control Conference, 2005. Proceedings of the 2005*, pp. 4690–4695, IEEE, 2005.

10. Huang, H., G. M. Hoffmann, S. L. Waslander and C. J. Tomlin, "Aerodynamics and control of autonomous quadrotor helicopters in aggressive maneuvering", *Robotics and Automation, 2009. ICRA'09. IEEE International Conference on*, pp. 3277–3282, IEEE, 2009.

11. Waslander, S. and C. Wang, "Wind disturbance estimation and rejection for quadrotor position control", *AIAA Infotech@ Aerospace Conference and AIAA Unmanned... Unlimited Conference*, p. 1983, 2009.

12. Hoffmann, G., H. Huang, S. Waslander and C. Tomlin, "Quadrotor helicopter flight dynamics and control: Theory and experiment", *AIAA Guidance, Navigation and Control Conference and Exhibit*, p. 6461, 2007.

13. Sydney, N., B. Smyth and D. A. Paley, "Dynamic control of autonomous quadrotor flight in an estimated wind field", *Decision and Control (CDC), 2013 IEEE 52nd Annual Conference on*, pp. 3609–3616, IEEE, 2013.

14. Tayebi, A. and S. McGilvray, "Attitude stabilization of a four-rotor aerial robot", *Decision and Control, 2004. CDC. 43rd IEEE Conference on*, Vol. 2, pp. 1216–1221, IEEE, 2004.

15. Dikmen, İ. C., A. Arisoy and H. Temeltas, "Attitude control of a quadrotor", *Recent Advances in Space Technologies, 2009. RAST'09. 4th International Conference on*, pp. 722–727, IEEE, 2009.

16. Zuo, Z., "Trajectory tracking control design with command-filtered compensation for a quadrotor", *IET control theory & applications*, Vol. 4, No. 11, pp. 2343–2355, 2010.

17. Madani, T. and A. Benallegue, "Backstepping control for a quadrotor helicopter", *Intelligent Robots and Systems, 2006 IEEE/RSJ International Conference on*, pp. 3255–3260, IEEE, 2006.

18. Zemalache, K. M., L. Beji and H. Marref, "Control of an under-actuated system: application a four rotors rotorcraft", *Robotics and Biomimetics (ROBIO). 2005 IEEE International Conference on*, pp. 404–409, IEEE, 2005.

19. Dunfied, J., M. Tarbouchi and G. Labonte, "Neural network based control of a four rotor helicopter", *Industrial Technology, 2004. IEEE ICIT'04. 2004 IEEE International Conference on*, Vol. 3, pp. 1543–1548, IEEE, 2004.

20. Tayebi, A. and S. McGilvray, "Attitude stabilization of a VTOL quadrotor aircraft", *IEEE Transactions on control systems technology*, Vol. 14, No. 3, pp. 562–571, 2006.

21. Raffo, G. V., M. G. Ortega and F. R. Rubio, "An integral predictive/nonlinear H∞ control structure for a quadrotor helicopter", *Automatica*, Vol. 46, No. 1, pp. 29–39, 2010.

22. Castillo, P., R. Lozano and A. Dzul, "Stabilization of a mini rotorcraft with four rotors", *IEEE control systems*, Vol. 25, No. 6, pp. 45–55, 2005.

23. Escareno, J., S. Salazar-Cruz and R. Lozano, "Embedded control of a four-rotor UAV", *American Control Conference, 2006*, pp. 6–pp, IEEE, 2006.

24. Kang, Y. and J. K. Hedrick, "Linear tracking for a fixed-wing UAV using nonlinear model predictive control", *IEEE Transactions on Control Systems Technology*, Vol. 17, No. 5, pp. 1202–1210, 2009.

25. Ogren, P., E. Fiorelli and N. E. Leonard, "Cooperative control of mobile sensor networks: Adaptive gradient climbing in a distributed environment", *IEEE Transactions on Automatic control*, Vol. 49, No. 8, pp. 1292–1302, 2004.

26. Porat, B. and A. Nehorai, "Localizing vapor-emitting sources by moving sensors", *IEEE Transactions on Signal processing*, Vol. 44, No. 4, pp. 1018–1021, 1996.

27. Murray, R. M. and S. S. Sastry, "Nonholonomic motion planning: Steering using sinusoids", *IEEE Transactions on Automatic Control*, Vol. 38, No. 5, pp. 700–716, 1993.

28. Zhang, C., D. Arnold, N. Ghods, A. Siranosian and M. Krstic, "Source seeking with non-holonomic unicycle without position measurement and with tuning of forward velocity", *Systems & control letters*, Vol. 56, No. 3, pp. 245–252, 2007.

29. Dobrokhodov, V. N., I. I. Kaminer, K. D. Jones and R. Ghabcheloo, "Vision-based tracking and motion estimation for moving targets using small UAVs", *American Control Conference, 2006*, pp. 6–pp, IEEE, 2006.

30. Campbell, M. E. and W. W. Whitacre, "Cooperative tracking using vision measurements on seascan UAVs", *IEEE Transactions on Control Systems Technology*, Vol. 15, No. 4, pp. 613–626, 2007.

31. Ariyur, K. B. and M. Krstic, *Real-time optimization by extremum-seeking control*, John Wiley & Sons, 2003.

32. Tan, Y., W. Moase, C. Manzie, D. Nešić and I. Mareels, "Extremum seeking from 1922 to 2010", *Control Conference (CCC), 2010 29th Chinese*, pp. 14–26, IEEE, 2010.

33. Liu, S.-J. and M. Krstic, *Stochastic averaging and stochastic extremum seeking*, Springer Science & Business Media, 2012.

34. Liu, S.-J. and M. Krstic, "Stochastic averaging in continuous time and its applications to extremum seeking", *IEEE Transactions on Automatic Control*, Vol. 55, No. 10, pp. 2235–2250, 2010.

35. Centioli, C., F. Iannone, G. Mazza, M. Panella, S. Podda, A. Tuccillo, V. Vitale, L. Pangione and L. Zaccarian, "Extremum seeking applied to the plasma control system of the Frascati Tokamak Upgrade", *Decision and Control, 2005 and 2005 European Control Conference. CDC-ECC'05. 44th IEEE Conference on*, pp. 8227–8232, IEEE, 2005.

36. Guay, M., D. Dochain and M. Perrier, "Adaptive extremum-seeking control of nonisothermal continuous stirred tank reactors", *Chemical Engineering Science*, Vol. 60, No. 13, pp. 3671–3681, 2005.

37. Becker, R., R. King, R. Petz and W. Nitsche, "Adaptive closed-loop separation control on a high-lift configuration using extremum seeking", *AIAA journal*, Vol. 45, No. 6, pp. 1382–1392, 2007.

38. Krieger, J. P. and M. Krstic, "Aircraft endurance maximization at medium mach numbers by extremum seeking", *Journal of Guidance, Control, and Dynamics*, Vol. 36, No. 2, pp. 390–403, 2013.

39. Tanelli, M., A. Astolfi and S. M. Savaresi, "Non-local extremum seeking control for active braking control systems", *Computer Aided Control System Design, 2006 IEEE International Conference on Control Applications, 2006 IEEE International Symposium on Intelligent Control, 2006 IEEE*, pp. 891–896, IEEE, 2006.

40. Cochran, J. and M. Krstic, "Nonholonomic source seeking with tuning of angular velocity", *IEEE Transactions on Automatic Control*, Vol. 54, No. 4, pp. 717–731, 2009.

41. Liu, S.-J. and M. Krstic, "Stochastic source seeking for nonholonomic unicycle", *Automatica*, Vol. 46, No. 9, pp. 1443–1453, 2010.

42. Cochran, J., A. Siranosian, N. Ghods and M. Krstic, "3-d source seeking for underactuated vehicles without position measurement", *IEEE Transactions on Robotics*, Vol. 25, No. 1, pp. 117–129, 2009.

43. Frihauf, P., S.-J. Liu and M. Krstic, "A single forward-velocity control signal for stochastic source seeking with multiple nonholonomic vehicles", *Journal of Dynamic Systems, Measurement, and Control*, Vol. 136, No. 5, p. 051024, 2014.

44. Ghods, N. and M. Krstic, "Speed regulation in steering-based source seeking", *Automatica*, Vol. 46, No. 2, pp. 452–459, 2010.

45. Rosero, E. and H. Werner, "Cooperative source seeking via gradient estimation and formation control (part 1)", *Control (CONTROL), 2014 UKACC International Conference on*, pp. 628–633, IEEE, 2014.

46. Isaacs, J. T., F. Quitin, L. R. G. Carrillo, U. Madhow and J. P. Hespanha, "Quadrotor control for RF source localization and tracking", *Unmanned Aircraft Systems (ICUAS), 2014 International Conference on*, pp. 244–252, IEEE, 2014.

47. Nikiforov, V. O., "Observers of external deterministic disturbances. II. objects with unknown parameters", *Automation and Remote Control*, Vol. 65, No. 11, pp. 1724–1732, 2004.

48. Chen, C.-T., *Linear system theory and design*, Oxford University Press, Inc., 1995.

49. Demircioglu, H. and H. I. Basturk, *Adaptive Controller for Quadrotor with Broken Propeller*, `https://goo.gl/nVsdsD`, accessed at May 2018.

50. Khalil, H. K., "Noninear systems", *Prentice-Hall, New Jersey*, Vol. 2, No. 5, pp. 5–1, 1996.

51. Bulgur, E. A., H. Demircioglu and H. I. Basturk, *Light Source Tracking with Quadrotor by Using Extremum Seeking Control* , `https://goo.gl/ukEp84`, accessed at May 2018.

52. Bulgur, E. A., H. Demircioglu and H. I. Basturk, *Light Source Tracking with Quadrotor* , `https://goo.gl/3MZEg9`, accessed at May 2018.

APPENDIX A: WIND DISTURBANCE CALCULATION

As seen in Figure 2.1, we describe 5 nodes on quadrotor where wind force affects. The wind velocity with respect to BFF on each node is given by

$$\begin{bmatrix} {}_iV_1 \\ {}_iV_2 \\ {}_iV_3 \end{bmatrix}_{BFF} = R \begin{bmatrix} {}_iV_{wind,x} \\ {}_iV_{wind,y} \\ {}_iV_{wind,z} \end{bmatrix}_{EFF} \tag{A.1}$$

for $i = 1:5$ describing the number of node where R is the rotation matrix, ${}_iV_{wind,x}$, ${}_iV_{wind,y}$, ${}_iV_{wind,z}$ are the wind velocity at i$^{\text{th}}$ node with respect to EFF found by using (3.124)–(3.126).

Based on (2.15), the drag forces and moments of wind on five nodes are given by

$$\begin{bmatrix} {}_iU_1 \\ {}_iU_2 \\ {}_iU_3 \end{bmatrix} = \frac{\rho C_D}{2} \begin{bmatrix} {}_iA_1 sign({}_iV_1)({}_iV_1^2) \\ {}_iA_2 sign({}_iV_2)({}_iV_2^2) \\ {}_iA_3 sign({}_iV_3)({}_iV_3^2) \end{bmatrix} \tag{A.2}$$

$$\begin{bmatrix} {}_iM_1 \\ {}_iM_2 \\ {}_iM_3 \end{bmatrix} = \begin{bmatrix} {}_id_1 \\ {}_id_2 \\ {}_id_3 \end{bmatrix} \times \begin{bmatrix} {}_iU_1 \\ {}_iU_2 \\ {}_iU_3 \end{bmatrix} \tag{A.3}$$

for $i = 1:5$ where U_i and M_i are the force and moment of wind disturbance affecting on i$^{\text{th}}$ node with respect to BFF, ${}_iA_1$, ${}_iA_2$, ${}_iA_3$, ${}_id_1$, ${}_id_2$, ${}_id_3$ are the areas and the distances to the center of i$^{\text{th}}$ node along B_1, B_2, B_3 respectively.

APPENDIX B: ERROR DYNAMICS

By substituting (2.4)–(2.6), (2.11)–(2.13) into (3.49), we can write the error terms in state space representation as

$$\begin{aligned}\dot{e}_1 =& Ae_1 + B\Big(- p_1\Omega_1^2 + p_2\Omega_2^2 + \epsilon_1 + s_\phi t_\theta(-p_3\Omega_3^2 + p_4\Omega_4^2 + \epsilon_2) + c_\phi t_\theta(q_1\Omega_1^2 + q_2\Omega_2^2 \\ & - q_3\Omega_3^2 - q_4\Omega_4^2 + \epsilon_3) + \kappa_1 - \ddot{\phi}_{des}\Big) \end{aligned} \tag{B.1}$$

$$\begin{aligned}\dot{e}_2 =& Ae_2 + B\Big(c_\phi(-p_3\Omega_3^2 + p_4\Omega_4^2 + \epsilon_2) - s_\phi(q_1\Omega_1^2 + q_2\Omega_2^2 - q_3\Omega_3^2 - q_4\Omega_4^2 + \epsilon_3) \\ & + \kappa_2 - \ddot{\theta}_{des}\Big) \end{aligned} \tag{B.2}$$

$$\begin{aligned}\dot{e}_3 =& Ae_3 + B\Big(\frac{s_\phi}{c_\theta}(-p_3\Omega_3^2 + p_4\Omega_4^2 + \epsilon_2) + \frac{c_\phi}{c_\theta}(q_1\Omega_1^2 + q_2\Omega_2^2 - q_3\Omega_3^2 - q_4\Omega_4^2 + \epsilon_3) \\ & + \kappa_3 - \ddot{\psi}_{des}\Big) \end{aligned} \tag{B.3}$$

$$\dot{e}_4 = Ae_4 + B\Big(c_\phi c_\theta(r_1\Omega_1^2 + r_2\Omega_2^2 + r_3\Omega_3^2 + r_4\Omega_4^2) + \epsilon_4 - g - \ddot{z}_{des}\Big) \tag{B.4}$$

where $A = \begin{bmatrix} 0 & 1 \\ 0 & 0 \end{bmatrix}$, $B = \begin{bmatrix} 0 \\ 1 \end{bmatrix}$ and

$$\epsilon_1 = \omega_2\omega_3\tau_1 + \beta_1^T\xi_1 + \beta_{p_1}^T\eta_{p_1} + \beta_{p_2}^T\eta_{p_2} + \beta_{\tau_1}^T\eta_{\tau_1} + \beta_1^T\delta_1 \tag{B.5}$$

$$\epsilon_2 = \omega_1\omega_3\tau_2 + \beta_2^T\xi_2 + \beta_{p_3}^T\eta_{p_3} + \beta_{p_4}^T\eta_{p_4} + \beta_{\tau_2}^T\eta_{\tau_2} + \beta_2^T\delta_2 \tag{B.6}$$

$$\epsilon_3 = \omega_1\omega_2\tau_3 + \beta_3^T\xi_3 + \beta_{q_1}^T\eta_{q_1} + \beta_{q_2}^T\eta_{q_2} + \beta_{q_3}^T\eta_{q_3} + \beta_{q_4}^T\eta_{q_4} + \beta_{\tau_3}^T\eta_{\tau_3} + \beta_3^T\delta_3 \tag{B.7}$$

$$\epsilon_4 = \beta_4^T\xi_4 + \beta_{r_1}^T\eta_{r_1} + \beta_{r_2}^T\eta_{r_2} + \beta_{r_3}^T\eta_{r_3} + \beta_{r_4}^T\eta_{r_4} + \beta_4^T\delta_4 \tag{B.8}$$